A thermodynamic and dynamic Lagrangian model for icebergs: A data-model intercomparison for the Southern Ocean

Maria Abrahamowicz

Master of Science

Department

McGill University

Montréal,Québec

August 2007

A thesis submitted to McGill University in partial fulfillment of the requirements of the degree of Master of Science

DEDICATION

I dedicate this thesis to my parents Basia and Michal, my sister Joasia and Rohan, for helping me, in all the best ways possible...

ACKNOWLEDGEMENTS

I would like to thank my supervisor, professor Bruno Tremblay, who guided me throughout this research project and introduced me to the world of icebergs. I would also like to highlight the financial help provided by the National Research Council. I also extend my thanks to all the people that patiently answered my numerous questions, particularly my neighbor Keith Ngan and professor Grant Bigg. I would also like to thank Michael Havas for keeping my computer 'Bergybit' alive and all the inhabitants of the 7th, 8th and 9th floor of Burnside Hall who provided uninterrupted occasions for stimulating (research) conversations. I am also grateful to reviewers, professor Stuart Savage and professor David Straub, for providing helpful suggestions on the modeling section of my thesis. Finally, I wish to thank Vaughn Thomassin, for his boundless resourcefulness and kindness.

ABSTRACT

A Lagrangian dynamic and thermodynamic iceberg drift model was developed, coded and validated against observations. First, the model was used to create a climatology (1979-2000) of iceberg drift in the Southern Ocean. The simulation reproduced the main patterns of motion and the northernmost extent of Antarctic icebergs as inferred from satellite and ship observations. The model was then used to hindcast 29 giant iceberg drift tracks in what was the first study of an iceberg model ability to reproduce the motion of individual icebergs *around the Antarctic continent on timescales of years*. The shape and timing of twelve of the twenty-nine tracks was successfully modeled with a model error in the 0.9-50% range. In six cases, the shape of the observed drift track was reproduced but the timing was off, and in the remaining eleven simulation the icebergs moved in the wrong direction. The model error was found to be independent of simulation length suggesting that the error was due to inaccuracies in the forcing data rather than in the physics of the model. In particular, model performance deteriorated in coastal areas and in the southern portions of the Weddell and Ross sea, highlighting the need for higher resolution forcing data in these regions. The model accuracy would benefit from a better definition of the Antarctic coastline, a better representation of Katabatic winds off the continent and a forcing ocean model which would include a dynamic and thermodynamic sea-ice component.

ABRÉGÉ

Un modèle Lagrangien dynamique-thermodynamique pour la dérive d'icebergs a été développé, codé et validé à l'aide d'observations. Premièrement, nous avons produit, à l'aide du modèle, une climatologie (1979-2000) de la dérive d'icebergs dans l'Océan du Sud. Les principales tendances du mouvement des icebergs simulés sont en accord avec les observations satellitaires et les mesures in-situ. Le modèle simule bien la limite septentrionale des icebergs d'Antarctique. Nous avons ensuite simulé vingt-neuf trajectoires individuelles d'icebergs géants. C'est la première fois qu'une telle étude est menée pour des icebergs observés *autour de l'Antarctique et sur une échelle de plusieurs années*. Dans douze cas, le tracé et le minutage de la trajectoire observée a été reproduit avec succès (erreur de 0.9-50%). Six simulations avaient des erreurs de temps mais non de trajet et dans les onze simulations restantes, l'iceberg a dérivé dans la mauvaise direction. Il a été établi que l'erreur du modèle était indépendante de la durée de la simulation, suggérant que l'erreur était due au champ de forçage plutôt qu'aux équations physiques du modéle. En particulier, une détérioration de la qualité des résultats a été observée dans les régions côtières et dans les parties sud des mers de Ross et de Weddell; soulignant ainsi le besoin d'améliorer le champ de forçage dans ces régions. D'autres moyens d'augmenter la précision du modèle seraient, entre autre, une meilleure définition de la géographie côtière de l'Antarctique, une meilleure représentation des vents catabatiques et un modèle océanique incluant une composante de glace dynamique et thermodynamique.

TABLE OF CONTENTS

LIST OF TABLES

LIST OF FIGURES

CHAPTER 1
Introduction

Antarctic icebergs rarely threaten shipping lanes or offshore structures - as do their Arctic counterparts - but, they still exert considerable influence over the Southern Ocean. Every year, roughly 2000 gigatons of ice break off from Antarctic ice sheets/shelves and glaciers in the form of icebergs (Jacobs et al., 1992). These icebergs then float away and melt in the Southern Ocean, releasing considerable amounts of freshwater and terrestrial sediments into the ocean (Silva et al., 2006; Jacka and Giles, 2007). The input of freshwater is believed to stabilize the polar ocean water column, influencing the production of Antarctic Deep and Intermediate water and, thus, the global overturning circulation (Lichey and Hellmer, 2001; Holland and Maqueda, 2004). The fine sediments melted out from the icebergs provide essential nutrients - such as iron - for the primary biological productivity (*e.g.,* growth of phytoplankton) of the Southern Ocean (Löscher et al., 1997). In fact, a recent study by Smith Jr. et al. (2007) suggests that icebergs behave as hot spots of continual micronutrient release and serve as areas of increased production and sequestration of organic carbon to the deep sea. The coarser sediments and, particularly ice-rafted-debris (IRD), are, on the other hand, deposited on the sea floor, creating layered sedimentary archives of the glacial activity of Antarctica. Likewise, grounded Antarctic icebergs can have a "profound and long-term impact"(Massom,

2003) on their surroundings, affecting amongst other "regional sea-ice extent, concentration, thickness distribution, drift patterns and ice production rates" (*e.g.,* by locking in fast-ice and leading to a dynamic thickening of the ice cover)(Massom, 2003) as well as the marine species - such as bryozoa or "moss animals" - living in its vicinity (Brey et al., 1999).

However, while Antarctic icebergs' influence on ocean dynamics, biological productivity, IRD deposition, sea-ice formation and the global carbon budget have all been documented, much less is known about the spatial extent of their impact. There is still little knowledge and/or consensus about, for example, the distribution of and magnitude of iceberg meltwater input in the Southern Ocean. Determining the melt and motion of Antarctic icebergs, and thus, delimiting the extent of their influence on the (geo-)physical and biological environment of the Southern Ocean is thus of great interest to the scientific community. A better knowledge of the patterns of drift and deterioration of Antarctic icebergs and of the above phenomena becomes more pressing in the current context of climate warming, amidst speculation of (1) (West) Antarctic Ice Sheet instability and future deglaciation (*e.g.,* Oppenheimer, 1998; Intergovernmental Panel on Climate Change, 2007) and (2) increasing number of icebergs in the Weddell Sea (Smith Jr. et al., 2007; Scambos et al., 2000).

Unfortunately, observational data of Antarctic icebergs is scarce. Because of the relative isolation of the Southern Ocean, aerial and ship-based monitoring of Antarctic icebergs is sporadic. The advent of satellites circa 1966 has allowed the tracking of giant icebergs - *i.e.,* of icebergs exceeding tens of kilometers in horizontal

dimension - but, the calving of giant icebergs is infrequent and their size *not* representative of Southern Ocean icebergs. In fact, the National Ice Center (NIC), which maintains a database of giant icebergs in the Southern Ocean, has to date (from 1979 to August 2007) reported only 124 icebergs. In contrast, during the Norwegian Antarctic Research Expedition (NARE) 1978-1979, 2119 icebergs were observed in the South Atlantic Weddell Sea region, and none exceeded one kilometer in diameter (Orheim, 1980). More generally, it is estimated that the Antarctic ice sheet produces tens of thousand of icebergs every year (Orheim, 1988; Silva et al., 2006). As for iceberg melt, in-situ and/or remote measurements are extremely rare, with most of our current knowledge of iceberg deterioration based on laboratory experiments and theoretical considerations rather than observations (Savage, 2002).

Thus, due to the lack of measurements, the current exploration of the dynamics and thermodynamics of icebergs relies heavily on numerical modeling. Unfortunately, in something akin to a Catch-22 scenario, numerical modeling relies on insufficient observational data for validation. In the following, we present a historical review of iceberg modeling, as well as the model validation studies done over the years.

1.1 Overview of iceberg drift modeling

Iceberg numerical modeling is a relatively new field which emerged in the 1970s. In its infancy, three approaches to iceberg modeling were proposed:(1) statistical methods, which use probability distributions of previously observed iceberg tracks to estimate iceberg drift, (2) kinematic methods, which relate iceberg drift speed and direction to other parameters (*e.g.,* wind speed) through empirical relationships, and (3) dynamic methods, which estimate the forces acting on an iceberg in order to

integrate the equation of motion (Hay and Company Consultants Inc., 1986; Smith, 1993). More recently, Holland and Maqueda (2004) and Schäfer-Neth and Stattegger (1999) have - respectively - argued for and against using an Eulerian approach to iceberg modeling. The Eulerian model, set in a fixed frame of reference, tracks the evolution of an iceberg-density function instead of tracking the drift of individual icebergs as is done in Lagrangian (moving frame of reference) models. Each method has its relative merits, reviewed amongst other by Hay and Company Consultants Inc. (1986), Marko et al. (1988), Schäfer-Neth and Stattegger (1999) and Clarke and La Prairie (2001). Nonetheless, of all these approaches, the dynamic method appears to be the favorite in both scientific and operational milieus, most probably because: (1) it is the most physical method, (2) it does *not* depend on voluminous amounts of hard-to-get iceberg observations and, (3) it provides the user with the most detailed output. In fact, by 1990s, the scientific modeling literature is almost exclusively concerned with the Lagrangian dynamic approach. For this reason, in this study, we limit our attention to "dynamic" iceberg models, also referred to as Iceberg Drift Models (IDMs); a term which we adopt in the following chapters.

The inclusion of a thermodynamic scheme in IDMs has not been systematic. Over the years, most short-timescale iceberg drift modeling studies have ignored iceberg melting assuming the berg deterioration to be negligible over a period of a few days (*e.g.,* Mountain, 1980; Sodhi and El-Tahan, 1980; Smith, 1993). More surprisingly, at least one study has also argued that iceberg melt is insignificant over a period of a few *years* (Lichey and Hellmer, 2001). The majority of long timescale iceberg studies have, however, included a thermodynamic scheme in their

models (*e.g.,* see Matsumoto, 1996, 1997; Bigg et al., 1996, 1997; Schäfer-Neth and Stattegger, 1999; Gladstone et al., 2001; Death et al., 2006). Unfortunately, as noted by Savage (2002) in his detailed review of IDMs, because of the lack of data and the wide range of fields that iceberg deterioration encompasses, the material on deterioration is much more ambiguous than the topic of drift. In fact, most of our knowledge of iceberg melt stem from a short-lived interest, during the 1970-1980s, in "harvesting" Antarctic icebergs for freshwater. During that period, a few "rather crude"(Savage, 2002) predictive equations for individual iceberg melt processes were developed based on a combination of laboratory experiments, iceberg population observations and theoretical consideration (*e.g.,* see Weeks and Campbell, 1973; Job, 1978; Russell-Head, 1980; Huppert, 1980; Neshyba and Josberger, 1980; Budd et al., 1980; Job, 1978; White et al., 1980). These equation form the basis of the most common thermodynamics scheme of present-day IDMs. They are either applied "as is" in the model (*e.g.,* see Bigg et al., 1996, 1997; Gladstone et al., 2001; Death et al., 2006) or used to determine a climatological iceberg life-expectancy, which is then implemented in the model (*e.g.,* see Matsumoto, 1996, 1997). Iceberg life-expectancy equations are region-specific and, so far, they have only been computed for the Grand Banks and Labrador Seas (Venkatesh and El-Tahan, 1988). Note that the set of thermodynamics equations currently being used are by no means complete as many important melt mechanisms, such as subsurface iceberg calving or fracture due to internal stresses, remain to be quantified.

1.2 IDMs and their application

Early iceberg drift modeling studies were motivated by a desire to limit iceberg hazard to shipping and offshore structures (*e.g.,* used in oil exploration) in the Arctic and North Atlantic Oceans. Specifically, the first IDMs were used to supplement plane, satellite and ship based observation of icebergs in the Northern waters. In fact, one of the first computerized iceberg drift model was developed in the 1970s for the International Ice Patrol, an organization consisting of 17 countries that has been monitoring iceberg danger in the Northwest Atlantic since 1912 (*i.e.,* two years after the fatal collision of the Titanic with an iceberg offshore of the Newfoundland Banks). The computerized IDM replaced the hand-plotted vector-addition model previously used by the Ice Patrol to predict iceberg motion in between iceberg aerial and ship-based reconnaissance operations (U.S. Coast Guard, 2003). In any case, because iceberg observations in the region of interest were (and still are) fairly frequent, the early IDMs were only used to forecast iceberg motion on short temporal and spatial scales. They also ignored iceberg melt. Accordingly, early iceberg drift modeling studies - which were mostly validation and sensitivity tests of the dynamic force balance - were limited to Northern waters and had spatial scales of a few degrees and time scales ranging from a few days to a month at most (*e.g.,* see Mountain, 1980; Sodhi and El-Tahan, 1980; Smith, 1993). We describe these early validation attempts in detail in section 1.3.1.

Then, in the 1990s, iceberg drift modeling shifted to larger spatial and temporal scales. Clarke and La Prairie (2001) point to the growing interest in (1) using ice-rafted-debris records to infer the past glacial activity of continental ice sheets,

(2) understanding the processes involved in iceberg sedimentation and (3) studying the impact of iceberg meltwater on ocean dynamics and, specifically, the global thermohaline circulation (THC) as main motivation behind the observed shift of focus.

Two first large-scale iceberg modeling papers were published in December 1996 by Bigg et al. (1996) and Matsumoto (1996), with their respective follow ups in April 1997 (Bigg et al., 1997; Matsumoto, 1997). In their studies, Bigg et al. (1996, 1997) combined the dynamic scheme of small-scale iceberg modeling studies with the melt parametrizations developed in the 1980s, in order to reproduce the ocean-wide North Atlantic iceberg field. The authors compared the model results with satellite, radar and ship-based observations of iceberg motion and density distribution, and also conducted sensitivity test of the IDM to forcing and other parameters (*e.g.,* ocean currents, launch dates, roll-over criterion etc.), in what was one of the first large-scale validation of IDMs. Details of their results is described in section 1.3.2.

Meanwhile, Matsumoto (1996, 1997) used a melt and drift IDM which also included a simple ice-rafted-debris (IRD) deposition subroutine to investigate iceberg sedimentation and meltwater flux in the North Atlantic Ocean. Matsumoto (1996) compared contemporaneous modeled IRD deposition patterns with IRD patterns from the last interglacial period (roughly 125 000 years ago). By the author's own account, his study involved a number of poorly constrained parameters (*e.g.,* the melt routine, the concentration of IRD in the model iceberg) and unverified assumption (*e.g.,* today's iceberg calving rates are a reasonable approximation for those of the last interglacial). Nonetheless, comparison of model and observation revealed enough

similarities between the two IRD fields for the author to conclude that the climate and, specifically, the surface ocean currents of the last interglacial were similar to today's. Based on simulations of iceberg meltwater flux, Matsumoto (1996) also suggested that iceberg freshwater input during the last interglacial was insufficient to trigger noticeable changes in the North Atlantic Deep Water circulation. In the second paper, Matsumoto (1997) examined iceberg sedimentation and melting under *glacial* conditions with the aim of testing the model's sensitivity to boundary conditions rather than reproducing the North Atlantic Ocean "glacial" IRD distribution. To this end, the author devised five numerical experiments in which he varied (1) the formulation of glacial iceberg decay, (2) the geographic extent of continental ice sheet (and thus, calving locations) and, (3) the ocean currents and wind fields. He found that ocean currents exerted by far the biggest influence on the overall pattern and rate of deposition of IRD. Winds, the iceberg melt routine and the location of calving sites also had a non-negligible but smaller impact.

The reasonable success in simulating the large scale drift of Arctic icebergs (Bigg et al., 1996, 1997) and the associated sedimentation and meltwater input (Matsumoto, 1996, 1997) opened the door to subsequent paleoclimate and ocean dynamics IDM studies. For instance, two years later, Schäfer-Neth and Stattegger (1999) carried out a numerical simulation of ocean circulation changes and IRD deposition rates in the North Atlantic Ocean and the Greenland-Iceland-Norwegian (GIN) seas during the Last Glacial Maximum (LGM). Even though the authors used a simplified model formulation, they were able to reproduce to some degree the thickness and extent of the Heinrich layers as seen in ocean cores collected in the northern

North Atlantic (*e.g.,* see Heinrich, 1988; Bond et al., 1992; Broecker et al., 1992). Heinrich layers are thick layers of IRD observed in marine sedimentary record in the North Atlantic resulting from massive recurrent iceberg discharge events (the Heinrich events) from continental ice sheets surrounding the Labrador Sea (*e.g.,* Clarke and La Prairie, 2001). There is still no consensus on the mechanism of these events nor on the magnitude of their impact. For instance, it has been suggested that the massive amount of freshwater release by the "Heinrich icebergs" could have affected the global thermohaline circulation, and triggered extreme climate events in the past (*e.g.,* Bond et al., 1993); thus, the interest in simulating not only iceberg sedimentation but also meltwater input in the Northern waters during the LGM. In Schäfer-Neth and Stattegger (1999)'s simulation, iceberg meltwater input during the LGM was comparable in magnitude to the direct meltwater runoff from continents. The authors suggested however that iceberg meltwater had a greater impact on the ocean circulation as it tended to be released further away from the coastline and at stronger rates in more narrow (sensitive) areas.

More recently, Death et al. (2006) revisited the problem of meltwater pulses during Heinrich events aiming to understand in more details the interplay between iceberg sedimentation and meltwater input during the LGM. Death et al. (2006) found the modeled sedimentation patterns *not* to be good proxies for the location and/or rates of iceberg meltwater input *if* modeled sediments were assumed to be

confined to the bottom portion of the iceberg[1] . Indeed, modeled icebergs continued to drift and melt much longer after all the basal debris was released *i.e.,* the distribution of iceberg meltwater extended much further from the coast than the distribution of IRD. More generally, the authors stated that while the presence of IRD in marine sediments usually indicates iceberg melt at that location, its absence cannot be interpreted as easily.

As just outlined, by the end of the 1990s, IDMs were frequently used to study the large scale behavior and impact of icebergs. Nonetheless, the first two large-scale iceberg drift modeling studies of *Antarctic* icebergs were only published in 2001. Gladstone et al. (2001) examined the ocean-wide scale motion and melt of contemporaneous Antarctic icebergs while Lichey and Hellmer (2001) used a dynamics-only IDM to hindcast the drift of a single giant iceberg monitored for over two years in the Southern Ocean. To the best of my knowledge, no other validation of IDMs in the Southern Ocean are currently available. Both studies are described in detail in the section below.

Finally, let us note that even though close to thirty years have elapsed since the implementation of the first operational IDM by the International Ice Patrol (IIP), small-scale iceberg drift modeling continues to be researched and improved. Recently, for example, the Canadian Ice Service (CIS) has been working to implement Savage

[1] Not much is known about the debris content of icebergs. Our current knowledge is based on a anecdotal observation of "dirty" icebergs and the quantitative analysis of small samples of debris-laden ice (*e.g.,* see Warnke and Richter, 1970; Anderson et al., 1980). Nonetheless, it is generally assumed that debris is preferentially confined to the lower parts of the icebergs (*e.g.,* see Drewry and Cooper, 1981; Dowdeswell and Dowdeswell, 1989; Dowdeswell and Murray, 1990)

(2002)'s numerical representation of the calving, drift and melt of bergy bits and growlers, in its operational IDM (Kubat et al., 2005). Bergy bits and growlers are small icebergs, less than 20 m in length, that are both too small to be detected by ship radar and too numerous to be modeled individually using IDMs. They are big enough however to cause significant damage to vessels hence the interest in modeling their (group) behavior (Savage, 2002).

1.3 IDM validation studies

1.3.1 Small-scale studies

All icebergs modeled in the four small-scale studies outlined in this section - mainly Mountain (1980), Sodhi and El-Tahan (1980), Smith (1993) and Kubat et al. (2005) - were located in the Northwest Atlantic, a region of commercial navigation and offshore exploration that is regularly monitored by the International Ice Patrol and the Canadian Ice Service during the iceberg season. Each study used a slightly different IDM but in all cases the thermodynamics of the iceberg were ignored and the following four forces were considered in the iceberg equation of motion; (1) the water form drag, (2) the wind form drag, (3) the Coriolis force, and (4) the pressure gradient force, also referred to as the sea surface tilt force (see Chapter 2 for details). Two models also allowed for added mass effects[2] (Sodhi and El-Tahan, 1980; Kubat et al., 2005). In all cases, the water drag was expressed as a vectorial sum of two or

[2] An object accelerating in a fluid, will also accelerate the fluid surrounding it. Because of an increased inertial drag, the object will then start to act as if mass was added to it. In the iceberg modeling literature, the added mass is usually taken to be half of the iceberg mass (Sodhi and El-Tahan, 1980; Kubat et al., 2005; Savage, 2002).

more layer of the water column to account for the variation of ocean currents with depth. Mountain (1980) relates the pressure gradient force to the geostrophic ocean currents while Sodhi and El-Tahan (1980), Smith (1993) and Kubat et al. (2005) also considered the water acceleration in their formulation of the force. In all cases, the model input included iceberg mass and size as well as wind and ocean current fields. The temporal resolution of the forcing data ranged from 12 hourly winds and climatological ocean currents with a spatial resolution on the order of 100 km and 40 km respectively (Mountain, 1980) to currents and winds measured continuously and within 1-20 km of the iceberg being tracked (Smith, 1993; Kubat et al., 2005).

Surprisingly, irrespective of the model and data differences, the broad conclusion of the four studies considered were similar. The main results are summarized as follows:

Validation against observations

Icebergs used in the validation tests ranged in size from small non-tabular to large tabular as defined in Table 1–1. Mountain (1980) and Sodhi and El-Tahan (1980) approximated observed iceberg dimension with the closest matching iceberg category of Table 1–1. Smith (1993) and Kubat et al. (2005) used observed iceberg size and shape information as is but all the values fell nonetheless within the above mentioned range.

In total, the drift of eighteen iceberg and one drogued buoy [3] was simulated and compared to observations (Mountain, 1980; Sodhi and El-Tahan, 1980; Smith, 1993; Kubat et al., 2005). In all cases, the model error was defined as the divergence between modeled and observed trajectory for a given time. All comparison showed good agreement between simulated and observed iceberg drift tracks. The model error of the shortest simulation (ranging from 11 hours to two days), which were also forced with higher spatial and temporal resolution data, did not exceed 14 km and usually remained below 5 km for total track lengths of 6-52 km (Sodhi and El-Tahan, 1980; Smith, 1993; Kubat et al., 2005). The much coarser forcing data and the longer duration (6 to 24 days) of Mountain (1980)'s simulation resulted in a model error in the 30-150km range for drift tracks in the 200-500 km range. In the later case, the error did not seem to be affected by drift duration which led Mountain (1980) to conclude that the model error was random and due to noisy forcing data rather than faulty model physics.

Sensitivity tests

Sensitivity test were conducted on a small subset of the icebergs used in the validation tests. A total of seven iceberg trajectories were tested, with only one of the drift tracks exceeding two days (Mountain, 1980). Note that Smith (1993) results should be interpreted with caution since the water and wind drag coefficients

[3] A drogued buoy is a buoy with a contraption that provides substantial resistance when dragged through the water.

Table 1–1: Arctic Iceberg Characteristics (Mountain, 1980, with acknowledgment to R.Q. Robe)

Size	Mass (10 kg^6)	Above-water area (m^2)	Submerged area (m^2) per depth layer			
			0-20m	20-50m	50-100m	100-120m
Non-tabular icebergs						
Growler	0.45	10	80	0	0	0
Small	75	230	780	820	0	0
Medium	900	910	1800	1900	2700	0
Large	5500	2000	3500	3750	5300	1400
Tabular icebergs						
Small	245	650	1 900	2 600	0	0
Medium	2 170	2 700	4 400	5 900	8 700	0
Large	8 235	5 200	7 200	9 700	14 400	5 000

were optimized independently for each sensitivity test, partially masking the effects of model and data variation.

Water Drag and Ocean Currents. The importance of water drag in governing iceberg drift is evident in numerical simulation of iceberg motion: IDMs are simply unable to simulate observed drift tracks when the water drag is artificially set to zero (Sodhi and El-Tahan, 1980; Kubat et al., 2005). The degree of detail of the water current used as input in the water drag calculation also impact model performance. Best results were obtained with a detailed water current profile (Mountain, 1980; Sodhi and El-Tahan, 1980; Smith, 1993; Kubat et al., 2005). Good results were also achieved when the water current profile was replaced with a weighted depth-averaged water current which took into account the size of the iceberg draft and its distribution within the different "velocity layers" of the water column (Kubat et al., 2005). In a test of three icebergs, a simple average of the water currents over a fixed depth of 100m, resulted in a 20-30% increase in the model error for the two bergs

with a draft shorter than 100m, and a marginal decrease in error (5%) for the iceberg with a draft deeper than 100m (Smith, 1993). Finally, when surface water currents (within the top 0-15m) were considered to be representative of the whole water column, the quality of the model prediction deteriorated very significantly (Sodhi and El-Tahan, 1980; Kubat et al., 2005).

Wind Drag. Both Sodhi and El-Tahan (1980) and Kubat et al. (2005) tested the IDM sensitivity to the inclusion and exclusion of the wind drag force. In two of the three iceberg trajectories considered, setting the wind drag to zero affected significantly model error. In the third case, the exclusion of the wind drag resulted in a negligible error increase.

Drag coefficients. Water and air drag forces are parametrized in terms of water/air velocity, area of iceberg exposed to the (water or wind) forcing and drag coefficients (see Section 2.2). Drag coefficients are dimensionless quantities which depend on the shape, size, inclination and roughness of the object under consideration as well as on the flow conditions. In practice, they are hard to measure. A standard approach has been to set the water and wind drag coefficient to values of 1 to 1.5, which are typically used for bluff bodies in a turbulent flow regime (Savage, 2002). Values ranging from 0.5 to 3.0 have nonetheless been tested (Mountain, 1980; Kubat et al., 2005) with negligible impact on model performance.

Smith (1993) has tried to optimize drag coefficient at the start of each run, allowing for values of 0.1-3.0 for the wind drag, and of 0.1-5.0 for the water drag, in the hope of finding characteristics coefficients for each modeled iceberg. But, the optimum coefficients varied widely throughout the simulation so that coefficients

fitted to and earlier part of a track were of no help in predicting the subsequent drift of a particular iceberg. When drag coefficient optimization was used to best fit the model to the observations – a technique which require an a priori knowledge of the entire iceberg trajectory under consideration – the mean optimum air and water drag coefficients were found to be 1.3 and 0.9 respectively (Smith, 1993).

Pressure Gradient Force. Two different formulation of the pressure gradient force (PGF) were tested. Mountain (1980), who estimated the PGF using a geostrophic ocean momentum equation, found that its exclusion led to a more erratic model error. Sodhi and El-Tahan (1980) showed that a slightly better model prediction was obtained when the PGF was rewritten using a non-geostrophic ocean momentum equation *i.e.,* including the water acceleration term. Finally, Smith (1993) mentions that while the exclusion of the water acceleration term, in the PGF formulation, will make the iceberg react less quickly to changes in water velocity, the resulting lag in response does not persist long enough to affect significantly the modeled drift. It might be however that, in Smith (1993)'s case, the lag was partially compensated by changes to the water drag coefficient.

Wave Radiation Force. The wave radiation force is the force imparted to a body by surface wave trains. Its magnitude depends on the way the waves are diffracted and dissipated by the body (Savage, 2002). Smith (1993) was the first to suggest the importance of the wave radiation force in governing iceberg motion. He also proposed a parametrization of the force that is still in use today. Yet, due to the lack of wave information, the force was not explicitly included in his model. According to the author, omission of the explicit wave force inflated the optimized

air drag coefficients by 40% on average. Using Smith (1993)'s formulation of the wave force, Kubat et al. (2005) found that the magnitude and impact of the force increased with increasing wave height. No attempt was however made by the authors to evaluate the influence of the wave radiation force on the predictive performance of the model due to lack of wave observation at the time of the iceberg tracking.

Iceberg Mass and Size. Iceberg size (cross-sectional areas) and mass were shown to have a strong effect on model performance by both Sodhi and El-Tahan (1980) and Kubat et al. (2005). Sodhi and El-Tahan (1980) reran model simulations of a *medium* non-tabular iceberg (as per Table1–1) using the iceberg characteristics of a *small*, and subsequently, a *large* non-tabular icebergs. The three simulated drift tracks diverged significantly, and the model error increased significantly when the "wrong" iceberg characteristics were used. Similarly, Kubat et al. (2005) found that relatively small variation in iceberg size and mass resulted in noticeably different simulated drift paths. It is not clear however if the observed effects are primarily due to changes in iceberg mass or size. It is of note that in both cases, the iceberg mass was already artificially augmented by half to reflect added-mass effects. Smith (1993), who did not consider added-mass effects in his model, ran test where an iceberg's mass was artificially doubled and quadrupled with no changes to its dimensions *i.e.,* only the density of ice was changed. The author observed no noticeable change in model results but, once again, the real effects of an increased iceberg mass might have been masked by the optimization of water and air drag coefficients.

Melt validation

In addition to the dynamics-only studies described above, a few small-scale deterioration-only validation studies have also been performed. Here we only outline tests of models consisting of parametric equation of individual iceberg deterioration mechanisms including: (1) wave erosion and calving of overhanging slabs, (2) forced water convection[4] , (3) buoyant vertical convection and, in some cases, (4) wind convection and (5) solar radiation (see Section 2.3 for detailed description of the terms). All studies were based in the North Atlantic Ocean during the summer-fall months (March to September). Time scales considered ranged from a few days (Hanson, 1988; Kubat et al., 2007) to several weeks (El-Tahan et al., 1987; Venkatesh et al., 1994).

The first and most thorough model validation was conducted by El-Tahan et al. (1987) who modeled the deterioration of three icebergs over a period of 4 to 25 days, taking into consideration all five mechanisms outline above. The predicted and observed iceberg mass losses showed good agreement. The iceberg mass at the end of each simulation was overestimated by approximately 10%. Comparison of the individual contribution of modeled deterioration mechanisms revealed that wave erosion

[4] Forced convection refers to heat advection by a fluid whose motion is not generated by buoyant forces, but rather an external source. The velocity difference between the iceberg and the ocean currents sets up a forced (water) convective circulation at the base of the iceberg, and results in the forced convection melting of the submerged portion of the iceberg (Savage, 2002). Note that the velocity difference between iceberg and wind similarly results in the forced (air) convection of the above-water portion of the iceberg. Forced air convection is however ignored in our model as its contribution to iceberg melt is very small compared to other deterioration mechanisms (Savage, 2002).

and calving were by far the most important terms (78% of total mass loss on average) followed by forced water convection (16%). Buoyant vertical convection, wind convection and solar radiation contributed less than 3% each. Based on simulations of four medium sized icebergs over five days, Hanson (1988) similarly found that the dominant deterioration process was wave erosion (amounting to roughly 4m day^{-1} of the total iceberg length) , with forced water convection (0.15m day^{-1}), buoyant vertical convection (0.07m/day^{-1}) and solar radiation (0.04m/day^{-1}) being the least important terms. These results were once again confirmed by Kubat et al. (2007) who simulated the deterioration of a generic iceberg under the influence of processes (1),(2),(3) and (5) – listed above – and found the deterioration rate associated with wave erosion and calving to be the greatest.

Kubat et al. (2007) further tested the wave erosion and calving equation by simulating mean calving intervals for iceberg in waters of a given temperature. Wave erosion erodes a notch in the iceberg at the waterline, creating an overhanging slab of ice. When the hanging slab of ice reaches a certain length (mass) bending stresses will cause it to break away (calve). Thus, a model's ability to predict a calving interval validates both the wave erosion and calving equations. The calving interval predicted by Kubat et al. (2007)'s model agreed well with estimates of calving intervals based on photo and video records of icebergs calving in the Canadian and Greenland waters from 1998 to 2005; in both cases the calving interval increased with decreasing water temperature. A few years before, Venkatesh et al. (1994) had also tried to validated the wave erosion and calving equations by hindcasting the time of calving of two satellite-tracked icebergs. However, while the predicted calving time agreed very

well with observations, the accuracy of the prediction hinged on the choice of surface water temperature which was crudely estimated or, perhaps more precisely, fitted to the data of their study. Moreover, the "observed" iceberg calving time was inferred from the loss (significant change) in satellite-tracked beacon used to monitor the icebergs rather than from direct observation of the event, an approach that Marko and Fissel (1995) judged to be "ambiguous and insufficient" in a comment piece of Venkatesh et al. (1994)'s study.

1.3.2 Ocean-basin scale studies

Arctic

In two companion papers, Bigg et al. (1996, 1997) conducted the first (and, so far, last) large-scale iceberg drift modeling study of contemporaneous North Atlantic and Arctic icebergs. At ocean-wide scales, the dynamics and thermodynamics of icebergs cannot be separated as there exist a continuous feedback between iceberg size and mass and its motion. As outlined in the previous section, even on timescales of days, the iceberg dimension can have a pronounced effect on its drift. Accordingly, Bigg et al. (1996, 1997)'s IDM included a thermodynamic scheme, which took into consideration wave erosion, forced convection, buoyant vertical convection, solar radiation as well as sensible heating, and sublimation. Icebergs were also allowed to roll-over. The formulation of the forced convection at the iceberg underside, and buoyant vertical convection processes followed El-Tahan et al. (1987). Because of lack of wave data, wave erosion was assumed to be a linear function of the Beaufort

wind force, as defined by the marine Beaufort scale[5] . The equation of motion used in the model took into account the water form drag, the wind form drag, the pressure gradient force, the Coriolis force, the wave radiation force as well as the sea-ice drag. The pressure gradient force was written as the sum of the water acceleration term and of the geostrophic term (see sections 1.3.1 and 2.3).

The model was forced with monthly atmosphere and ocean forcing fields taken from an atmospheric and oceanic general circulation model (GCM) respectively. Note that the ocean model did not include a sea-ice component. The ocean variables had 1° horizontal resolution, and 19 vertical levels. However, only the *surface* fields were used in the simulations, even though the modeled iceberg drafts ranged from 67 to 300m. Bigg et al. (1997) justifies his choice by stating that the "upper two or three levels in the ocean model tended to have similar properties over the region in which icebergs are found", with no additional information on either the extent of the similitude or the depth corresponding to these "upper two or three" ocean levels. Finally, monthly sea-ice fields were digitized from the Bourke and Garrett (1987) climatology of Arctic sea-ice thicknesses. Note that the sea-ice drag was parametrized as function of sea-ice thicknesses and velocity (taken to be that of surface water currents). Sea-ice concentration was not considered. Linear interpolation was used to interpolate between the monthly average forcing fields. Iceberg calving rates and

[5] The marine Beaufort scale is used to infer wind speed from the observed sea conditions and wave heights. It consist of thirteen wind force categories that range from 0, for a flat sea and winds of 0-0.2m s^{-1}, to 12, for a sea of huge waves that is completely white with driving spray, and winds of 33-41m s^{-1} (Wikipedia, 2007).

size distribution at each calving location (36 in total) were roughly estimated based on observation and empirical equations. The model was integrated until all modeled icebergs had melted away.

Comparisons of the general patterns of motion, of the southern limits and of the average life expectancies of modeled icebergs agreed well with descriptions/observations of these parameters available in the Arctic iceberg literature. As an aside, let us note that because of the strong interaction between iceberg melt and motion at larger scales, an IDMs ability to reproduce the motion of icebergs also confirms the model's ability to predict iceberg melt except in the (improbable) case where iceberg drift and melt errors systematically cancel out. The authors did not attempt to reproduce the drift of any real iceberg, ruling out from the start the model's ability to hindcast the drift of an observed iceberg over a period of a few years because of high model-sensitivity to forcing input amongst other. Indeed, Bigg et al. (1997) tried varying (1) the resolution of the ocean forcing fields, (2) the launch dates of the icebergs, and (3) the roll-over criterion and in all three cases, while the overall patterns of iceberg motion remained similar, the individual trajectories diverged significantly.

The authors also examined the relative importance of the dynamic and thermodynamic terms. Together, the water form drag and the pressure gradient force were found to provide $70 \pm 15\%$ of the total dynamic forcing. Within the pressure gradient force, it was the water acceleration term rather than the geostrophic term that dominated. The Coriolis force and the air drag each accounted for roughly 15% of the total iceberg acceleration. The contribution of the wave radiation force was less than 5% and that of the sea ice drag, negligible in most cases.

In Bigg et al. (1997)'s study, wave erosion was the dominant melt term amounting to more than 1m day^{-1} of the iceberg length and width, in regions of strong winds. The forced convection was found by the authors to be of a comparable magnitude to the wave erosion melt, when water temperatures were above zero. Note that the forced convection affects the iceberg thickness rather than its length. Melting due to buoyant convection was negligible, except in waters several degrees above zero, in which case buoyant convection melting was as much as 0.2m day^{-1} of the iceberg length. Solar radiation, sensible heating and sublimation were found to be negligible no matter the forcing.

The magnitude of the forced convection melt in Bigg et al. (1997)'s simulations is much bigger than previously suggested. Indeed, results from small-scale melt studies seem to indicate that forced convection at the iceberg underside is usually an order of magnitude smaller than wave erosion and in no case comparable (see section 1.3.1). Forced convection at the iceberg underside is written in terms of a constant of proportionality, the relative velocity of water past the iceberg, and the temperature difference between water and ice surface. The relatively large contribution of Bigg et al. (1997)'s forced convection term might be due to the authors' use of surface ocean currents as input in the computation of a melt process that should consider the currents at the base of the iceberg, that is at depth as great as 300m in the author's simulations. Moreover, while previous small-scale melt studies have estimated the surface ice temperature to be 0℃(El-Tahan et al., 1987), -1℃(Hanson, 1988; U.S. Coast Guard, 2003) or roughly -2℃(Kubat et al., 2007), Bigg et al. (1997) have

taken it to be -4℃, which once again might have inflated the magnitude of the forced convection term in their study.

More generally, Bigg et al. (1997) use of surface water properties as an approximation of the properties of the water column up to depths of 300m may not be appropriate given that small-scale iceberg drift modeling studies have shown that replacing the depth-profile of water currents by surface currents leads to a dramatic decrease in model performance for iceberg as shallow as 67m (see section 1.3.1). Among other, we expect this substitution to strongly influence the water drag force, which is usually the dominant term in iceberg motion.

Antarctic

Gladstone et al. (2001) were the first to investigate the large-scale drift and melt patterns of contemporaneous icebergs in the Southern Ocean. To this end, the authors used a slightly modified version of Bigg et al. (1997)'s IDM. The formulation of the air and water drag forces was altered to include skin drag *i.e.,* the drag of wind/water on the berg's horizontal top/basal surface. Antarctic icebergs are much more tabular in shape than Arctic icebergs; one thus expect skin drag to be much more important for the former. Using a scaling argument, the authors also discarded the water acceleration term from their formulation of the pressure gradient force. Finally, the wave erosion equation of Bigg et al. (1997) was refined to include a simple temperature dependency.

The simulation was run with monthly reanalysis winds of 1.125° resolution. The ocean fields were taken from a seasonal average of a four-year climatological run of the high resolution (0.25°) OCCAM ocean model, which did not include a sea-ice

component. The top seven levels (roughly 180m) of the ocean model were then averaged to calculate the seasonal depth-averaged ocean currents and temperatures. Sea-ice concentrations were digitized from satellite data at a 2° resolution. Lastly, an extra 10m s^{-1} was added to the winds at a $2\frac{1}{2}$ day cycle – 12 hours eastward, 12 hours northward, 12 hours westward, 12 hours southward and 12 hours of no extra forcing – to simulate the passage of mesoscale weather systems. Calving sites (29 in total), calving fluxes and size distribution of icebergs at a given location were estimated from observations. In terms of shape, icebergs were assumed to remain tabular and maintain a constant length to width ratio. Giant icebergs - defined as icebergs with horizontal extent of at least 10 nautical miles (roughly 18.5 km) were not considered in the simulation even though they are thought to account for as much as half the total Antarctic iceberg calving flux (Jacobs et al., 1992).

Model results show fairly good agreement with the large-scale motion patterns inferred from the few satellite, radar and ship based observations of Antarctic icebergs available in the literature. Amongst other, the simulated iceberg trajectories reproduced the three main modes of Antarctic icebergs motion as diagnosed from satellite observation by Tchernia and Jeannin (1984), mainly: (1) near the coast, icebergs drift westward in the Antarctic Coastal Current, (2) icebergs tend move away from the coast in specific zones known as retroflection zones, and (3) away from the coast, icebergs move eastward with the Antarctic Circumpolar Current. Moreover, the simulated northern limits of icebergs show some similarities with observations.

Gladstone et al. (2001) also investigate the sensitivity of the simulated drift of "regular sized" icebergs (horizontal extent of 10^2-10^3m) to various forcing terms. The

water and air drag forces were found by the authors to exert the strongest influence on iceberg motion. Both forces were of similar magnitude while the wave radiation, Coriolis and pressure gradient forces were roughly an order of magnitude smaller, and the sea-ice drag typically two orders of magnitude smaller. The authors note however that the importance of the Coriolis and pressure gradient forces increases with increasing iceberg mass. Moreover, both forces need to be included in the IDM for the model to be able to reproduce the coastal westward drift and the retroflection zones characteristic of large-scale Antarctic iceberg motion. Indeed, when both the Coriolis force and the pressure gradient force are set to zero, the model runs show northward motion all around the Antarctic continent and very little coastal drift. The extra mesoscale forcing also influences coastal iceberg motion. By introducing small meanders in the simulated iceberg drift trajectories, this extra forcing allows a greater proportion of modeled icebergs to leave the coastal current then when no extra forcing is applied. Finally, as in Bigg et al. (1997), the most important melt terms are found to be wave erosion and forced convection.

The only other large-scale IDM validation of Antarctic iceberg drift was done by Lichey and Hellmer (2001). The authors used a dynamics-only IDM to hindcast the drift of a giant iceberg (iceberg C7), with a particular emphasis placed on understanding the influence of sea-ice on iceberg motion. Iceberg C7 was tracked by satellite over a period of two years, during which it slowly crossed the Weddell Sea, a region characterized by high sea-ice concentration and multi-year ice year-round (see figures A–5 and A–6).

In Lichey and Hellmer (2001)'s model, iceberg motion is governed by the full (form and skin) water and air drag forces, the Coriolis force, the pressure gradient (sea slope) force, and the sea-ice drag. The pressure gradient force is rewritten in terms of the tilt angle of the sea slope, itself estimated from the barotropic part of the modeled ocean velocity. The sea-ice drag is split into three sea-ice concentration categories;(1) for concentration of less than 15%, the sea-ice drag is set to zero, (2) for values of 15-90% the sea-ice drag is computed as a normal drag force and (3) for concentration greater than 90%, and provided that some critical value of sea-ice strength P_s = 13000N m^{-1} is met, the iceberg is assumed to drift at/with sea-ice velocity. The sea ice strength is parametrized as a function of sea ice concentration and thickness. The sea-ice concentration, thickness and velocity data is taken from a stand-alone dynamic-thermodynamic sea-ice/mixed-layer model that does not include the iceberg.

The model is forced using coarse spatial resolution ocean currents, which are vertically integrated over the first 200m of the water column; a depth which roughly corresponds to the estimated draft thickness of iceberg C7 (250m). The winds are taken from the NCEP reanalysis. Both wind and ocean fields have a temporal resolution of 3 days. The modeled C7 iceberg is box-shaped, with a 28×28km horizontal surface. The authors ran several simulations with the iceberg launch position displaced by 0.2° meridionally each time, from a starting latitude of 70°S up to 67.8°S. All runs were integrated for slightly more than two years to match the duration of the observational record. Note that no change in C7's horizontal size was recorded during the observation period, which partially justifies the authors omission of iceberg thermodynamics in their model. Thickness information is not included in the

iceberg dataset used by Lichey and Hellmer (2001), so it is unclear if the exclusion of iceberg melt has resulted in an overestimation of the iceberg thickness during the two year model integration.

The authors first tested the sensitivity of the drift trajectory to the threshold sea-ice strength value used in their parametrization of the sea-ice drag. Best fit between modeled and observed drift track was obtained when icebergs were assumed to "lock" with sea-ice at a threshold ice strength corresponding to an ice thickness of 0.8-1m and a concentration of 84-100%. This threshold value was used in subsequent tests of the relative importance of the wind, water and sea-ice drag forces in governing iceberg motion. Lichey and Hellmer (2001) found that running the model without a wind force drag resulted in only a minor deterioration of the simulated drift tracks. Similarly setting the ocean currents to zero had very little impact on the simulated trajectories, which were almost identical to model runs with non-zero ocean currents. On the other hand, setting the sea-ice drag to zero resulted in a dramatic deterioration of model performance. According to Lichey and Hellmer (2001), the sea-ice "collects" the wind momentum that would otherwise be transferred to the ocean explaining the strong dominance of the sea-ice drag over the water drag in the region.

Lichey and Hellmer (2001) results are in contradiction with those of Bigg et al. (1997) and Gladstone et al. (2001) who both found sea-ice to exert the smallest influence on iceberg motion. However, both Bigg et al. (1997) and Gladstone et al. (2001) assumed sea-ice to move at the speed of surface currents. Moreover, Bigg et al. (1997) did not consider sea-ice concentration in his formulation of sea-ice drag

while Gladstone et al. (2001) used only a crude estimation of sea-ice thickness. These assumptions might have led to an underestimation of the importance of sea-ice drag in governing iceberg motion. More importantly, Bigg et al. (1997) and Gladstone et al. (2001) results were based on ocean-basin wide simulations of several hundreds of icebergs, many of which drifted in the open ocean, while Lichey and Hellmer (2001) only considered a few model icebergs drifting in the very high sea-ice concentration/thickness region that is the southern portion of Weddell Sea. Together, the three studies suggest that sea-ice drag is usually negligible, but can become very important locally. Finally, note that the decrease of the importance of the water and air drags relative to the sea-ice drag in Lichey and Hellmer (2001)'s study might have been influenced by the authors choice of water and air drag coefficient; the form-drag coefficients (0.4 for air, and 0.85 for water) are roughly half of the values generally used in the iceberg modeling literature, and the skin-drag coefficient (2.5×10^{-4} for air and 5.5×10^{-4} for water), an order of magnitude smaller.

1.4 Objectives and Thesis Overview

The importance of the determining the melt and motion of Antarctic icebergs is undeniable given their wide-ranging influence on the (geo-)physical and biological environment of the Southern Ocean. Due to the difficulties of observing and monitoring iceberg melt and motion, the study of icebergs relies heavily on iceberg drift models. Up to now, only two iceberg drift modeling studies of Antarctic icebergs have been published. The first study explores the general patterns of Antarctic iceberg motion and melt without, however, validating the model against any individual iceberg drift tracks (Gladstone et al., 2001) while, in the second study, an iceberg

drift model is validated against the drift of a single iceberg (Lichey and Hellmer, 2001). More generally, previous iceberg modeling studies have looked at IDM ability to either forecast the drift of individual icebergs, or reproduce the climatology of iceberg behavior.

Here, building on previous work, we intend to assess the ability of a single IDM to both (1) simulate the large-scale patterns of Antarctic iceberg drift, and (2) hindcast the drift of individual iceberg trajectories *around the Antarctic continent on timescale of years*.

Chapter 2 discusses the formulation of, and the numerical procedure used in our iceberg drift model. The model ability to simulate the large-scale drift patterns of Antarctic iceberg, as well as, the drift of individual (giant) icebergs is described in Chapter 3. Finally, Chapter 4 provides a general summary of the results and suggestions for future work.

CHAPTER 2
Model and Forcing

2.1 Iceberg Model

The iceberg drift model used in this study was developed and coded from scratch. Individual icebergs are modeled as point particles with finite area. They are cylindrical in shape at the time of calving and retain their shape as they melt. All shape-dependent calculations in this model use the *normal* area exposed to a given force, which, for cylindrical berg, will be isotropic. For comparison, in Gladstone et al. (2001), model Antarctic icebergs were taken to be box-shaped, and constrained to travel with their long axis parallel to water flow.

The initial iceberg diameter and thickness can be varied at will, and the iceberg mass and dry-wet ratio are computed on the fly. We favor this approach over iceberg size classes - which distinguish between a dozen or so iceberg sizes, each with a fixed mass and dry-wet ratio (*e.g.,* Mountain, 1980; Sodhi and El-Tahan, 1980; Matsumoto, 1996; Bigg et al., 1997; Death et al., 2006) - as it facilitates sensitivity studies on iceberg dimension/mass, and comparisons with icebergs of known dimensions.

As an aside, note that throughout this thesis, we will use the International System of Units (SI) (Table 2–1) unless explicitly stated otherwise. One exception is temperature, which is in degree Celsius (℃). All physical parameters and constants used in the equations of this chapter (and in the simulations) are listed in Table 2–2.

Table 2–1: Relevant SI base units and a few examples of derived units

Base quantity	Name	Symbol
Length	Meter	m
Mass	Kilogram	kg
Time	Second	s
Derived Quantity	**Name**	**Symbol**
Area	Square meter	m^2
Speed, velocity	Meter per second	$m\ s^{-1}$
Mass density	Kilogram per cubic meter	$kg\ m^{-3}$

Table 2–2: Physical parameters and constants used in the simulation

Symbol	Description	Value	Units
ρ_w	Density of ocean water	1027.5	$kg\ m^{-3}$
ρ_a	Density of air	1.3	$kg\ m^{-3}$
ρ_{pi}	Density of "pure" ice (and sea-ice)	905.0	$kg\ m^{-3}$
c_w	Form drag coefficient of water	1.0	-
c_a	Form drag coefficient of air	1.5	-
c_{si}	Form drag coefficient of sea-ice	1.0	-
c_{dw}	Skin drag coefficient of water	5.5×10^{-3}	-
c_{da}	Skin drag coefficient of air	1.2×10^{-3}	-
g	Gravitational acceleration	9.81	$m\ s^{-2}$
T_{ice}	Iceberg surface temperature	-1.8	℃
R	Ice roughness height	0.01	m
Pr	Prandtl number for sea-water at 0℃	13.4	-
k	Thermal conductivity for sea-water at 0℃	0.563	$kg\ m\ s^{-3}\ ℃^{-1}$
ν	Kinematic viscosity for sea-water at 0℃	1.83×10^{-6}	$m^2\ s^{-1}$
L_f	Latent heat of fusion of ice	3.34×10^5	$m^2\ s^{-2}$
F	Fetch length of wind	500 000	m

In this model, the iceberg mass is calculated using an empirical density profile $\rho_i(z)$ based on observations reported in Mellor (1961) and Orheim (1980):

$$\rho_i(z) = \begin{cases} 41.5\sqrt{z} + 500.0 & \text{if } z < 95m \\ \rho_{pi} & \text{if } z \geq 95m \end{cases} \tag{2.1}$$

where z is the vertical coordinate for iceberg depth - with $z = 0$ corresponding to the iceberg top - and ρ_{pi} is the density of "pure" ice. The gradual increase, and subsequent leveling off of the iceberg density with depth reflects the glaciological properties of Antarctic icebergs: observations show that Antarctic icebergs are made of increasingly dense layers, starting with layers of compressed (and partially melted) snow at the top, followed by layers of "ice with air bubbles" and finally, at depths greater than roughly 90-100m, layers of (almost) pure ice (*e.g.,* Mellor, 1961; Orheim, 1980; Wadhams, 2000). The vertical density profile expressed in 2.1 is integrated over the iceberg volume V to find the iceberg mass M:

$$M = \int_0^V \rho_i(z) dV = \int_0^h \rho_i(z) \pi R^2 dz \tag{2.2}$$

where h and R are the iceberg thickness (or "height") and radius respectively. The average density $\overline{\rho_i}$ of any given berg:

$$\overline{\rho_i} = \frac{1}{h} \int_0^h \rho_i(z) dz \tag{2.3}$$

is used to find the fraction of the iceberg lying below the surface of the water *i.e.,* the dry-wet ratio. Assuming that the iceberg is floating in static equilibrium in an

ocean of constant density ρ_w, the Archimedes principle states:

$$\underbrace{\overline{\rho_i} V_i g}_{\text{weight of the iceberg}} = \underbrace{\rho_w V_w g}_{\text{upward buoyant force acting on ice}} \tag{2.4}$$

where $g = 9.81\text{m s}^{-1}$ is the gravitational acceleration constant, and V_i and V_w are the volumes of the iceberg and of the displaced water respectively. Rearranging 2.4 gives:

$$r = \frac{V_w}{V_i} = \frac{\overline{\rho_i}}{\rho_w} \tag{2.5}$$

where r is the fraction of the iceberg lying below water. Equations for iceberg freeboard (above-water thickness) h_f and draft (below-water thickness) h_d follow directly from 2.5:

$$h_f = (1 - r) \times h = h - h_d \tag{2.6}$$

$$h_d = r \times h = h - h_f. \tag{2.7}$$

Note that as the iceberg thickness (h) increases, so does the average density ($\overline{\rho_i}$) and the fraction of ice below water (r) reflecting observation which show that thinner icebergs have a higher freeboard-to-thickness ratio than thicker icebergs (Orheim, 1980; Weeks and Mellor, 1978). Previous authors using "simple geometry" model icebergs (*e.g.,* cylindrical or box-shaped) have considered icebergs with a constant density (of pure ice) throughout, and have also fixed the dry-wet ratio to be constant at values of 1:5 (*e.g.,* Bigg et al., 1996, 1997) or even 0:1 (*i.e.,* no freeboard) (*e.g.,* Schäfer-Neth and Stattegger, 1999). The approach mentioned above is preferable since: (1) iceberg mass determines the strength of the Coriolis force, which is an

important driving force in iceberg motion, and (2) the dry-wet ratio affects the repartition of the air (dry) and water (wet) drags, which are generally the leading terms governing iceberg drift.

2.2 Dynamics

The momentum balance equation describing the motion of an iceberg of mass M drifting with horizontal velocity $\mathbf{u_i}$ is:

$$M\frac{d\mathbf{u_i}}{dt} = -Mf\hat{\mathbf{k}} \times \mathbf{u_i} + \mathbf{F_{ss}} + \mathbf{F_r} + \mathbf{F_w} + \mathbf{F_a} + \mathbf{F_{si}} \tag{2.8}$$

where t is the time; f is the Coriolis parameter; $\mathbf{F_{ss}}$ is the sea surface tilt force; $\mathbf{F_r}$ is the wave radiation force; and $\mathbf{F_w}$, $\mathbf{F_a}$, $\mathbf{F_{si}}$ are the water, air and sea-ice drag forces respectively. A similar balance of forces has been used as early as 1979 by the International Ice Patrol (see chapter 1),with the parametrization of individual terms refined over time by Smith (1993); Bigg et al. (1996); Gladstone et al. (2001); Lichey and Hellmer (2001) amongst other.

Sea Surface Tilt Force, $\mathbf{F_{ss}}$. Uneven heating, salinity variations, and currents, especially near boundaries (*e.g.*, coastal regions or ice shelves) can lead to a depression or protrusion of the ocean surface level relative to the geoid[1] . The resulting tilt of the sea surface causes a horizontal pressure gradient force, which influences iceberg motion. The sea surface tilt force is expressed as:

$$\mathbf{F_{ss}} = -Mg\nabla\eta \tag{2.9}$$

[1] The geoid is defined as the surface over which the gravitational potential is constant (Wadhams, 2000).

where η is the sea surface dynamic height. A second-order Taylor approximation, based on the sea surface height at the six grid points closest to the iceberg location, is used to calculate the zonal and meridional derivatives of sea surface height.

Wave Radiation Force, $\mathbf{F_r}$. The wave force is a function of the square of the amplitude of waves hitting the vertical sides of an iceberg. Wave information is however seldom available in climatological datasets/model runs. Bigg et al. (1997) have avoided this problem by rewriting the wave amplitude in terms of wind speed, based on data in the marine Beaufort scale. Following the authors' approach, the wave equation becomes:

$$\mathbf{F_r} = \frac{(0.02025)^2}{16}\rho_w g L |\mathbf{u_a}|^3 \mathbf{u_a} \tag{2.10}$$

where ρ_w is the density of ocean water, $\mathbf{u_a}$ is the wind velocity and L is the length of the berg normal to "incident" waves. In our model, L is simply the iceberg diameter D. Note that expression 2.10 does not account for the presence of ice cover (partial or otherwise), the resultant wave damping and effective reduction of the wave radiation stress.

Wind Drag, $\mathbf{F_a}$. The wind drag is expressed as a sum of a form drag (acting on above-water vertical walls of the iceberg) and a skin drag (acting on the iceberg top):

$$\begin{aligned} \mathbf{F_a} &= \underbrace{\frac{1}{2}(\rho_a c_a A_{va})|\mathbf{u_a} - \mathbf{u_i}|(\mathbf{u_a} - \mathbf{u_i})}_{\text{form drag}} + \underbrace{(\rho_a c_{da} A_{ha})|\mathbf{u_a} - \mathbf{u_i}|(\mathbf{u_a} - \mathbf{u_i})}_{\text{skin drag}} \\ &= [\frac{1}{2}(\rho_a c_a A_{va}) + (\rho_a c_{da} A_{ha})]|\mathbf{u_a} - \mathbf{u_i}|(\mathbf{u_a} - \mathbf{u_i}) \end{aligned} \tag{2.11}$$

where ρ_a is the density of air; $c_a = 1.5$ is the dimensionless form drag coefficient; $c_{da} = 1.2 \times 10^{-3}$ is the dimensionless skin drag coefficient of air, and A_{va} and A_{ha} are the cross-sectional and horizontal (top) iceberg areas exposed to wind respectively .

Water Drag, $\mathbf{F_w}$. Water drag is also written as a sum of drag forces acting on the submerged vertical wall of the iceberg (form drag) and on the iceberg base (skin drag). Because previous iceberg drift modeling studies (see chapter 1) have shown that best IDM performance is obtained with a detailed water current profile as input, we sum the water drag over all the discrete (model) ocean layers in which a given iceberg lies. The water drag force is thus given by

$$\mathbf{F_w} = \underbrace{\frac{1}{2}\rho_w c_w \sum_{k=1}^{n} [A_k |\mathbf{u_w^k} - \mathbf{u_i}|(\mathbf{u_w^k} - \mathbf{u_i})]}_{\text{form drag}} + \underbrace{(\rho_w c_{dw} A_{hw})|\mathbf{u_w^n} - \mathbf{u_i}|(\mathbf{u_w^k} - \mathbf{u_i})}_{\text{skin drag}} \quad (2.12)$$

where k is the vertical index of the kth water layer, with $k = 1$ corresponding to the surface ocean layer and $k = n$, to the deepest layer in which a given iceberg bathes; $\mathbf{u_w^k}$ and A_k are respectively the water velocity of the kth layer and the cross-sectional area of the iceberg in that layer; $c_w = 1.0$ is the dimensionless form drag coefficient; $c_{dw} = 5.5 \times 10^{-3}$ is the dimensionless skin-drag coefficient of water; $\mathbf{u_w^k}$ is the water velocity in the nth ocean-layer *i.e.,* the deepest ocean layer in which the iceberg lies, and A_{hw} is the horizontal surface area (base) exposed to the water flow.

Sea Ice Drag, $\mathbf{F_{si}}$. Sea-ice acts as a drag force in the iceberg's equation momentum equation at *all* sea-ice concentrations greater than 15%, such that

$$\mathbf{F_{si}} = \begin{cases} 0 & \text{if } Ci \leq 15\% \\ \frac{1}{2}(\rho_{pi} c_{si} A_{si})|\mathbf{u_{si}} - \mathbf{u_i}|(\mathbf{u_{si}} - \mathbf{u_i}) & \text{if } Ci > 15\% \end{cases} \quad (2.13)$$

where Ci (in percent %) is the sea-ice concentration; ρ_{pi} is the sea ice ("pure" ice) density; $\mathbf{u_{si}}$ and $c_{si} = 1.0$ are the sea ice velocity and form-drag coefficient respectively, and A_{si} is the product of the iceberg diameter and the sea-ice thickness.

The sea-ice drag as expressed in 2.13 is modified from Lichey and Hellmer (2001), who split the force due to sea-ice into three categories of sea-ice concentration. In their study, sea-ice acts as an additional drag force on the iceberg only if the sea-ice concentration is between 15 and 90%. Otherwise, at a concentration of less than 15%, the authors assume that the iceberg is floating in an open water environment and the sea-ice is set to zero. Whereas, at a concentration of more than 90% – and provided that some critical value of sea-ice strength is met – "iceberg and sea ice [are assumed to] form a solid block"(Lichey and Hellmer, 2001), in which case the iceberg does not accelerate but drifts at/with sea-ice velocity.

Joint motion of iceberg(s) and sea-ice has been observed, amongst others by Schodlok et al. (2005). Based on two one-year sets of iceberg and sea-ice buoy data, Schodlok et al. (2005) found coherent sea-ice iceberg movement to occur at sea-ice concentrations greater than 86% and 95%, with an associated length scale of coherent movement of 250 km and 150 km respectively. The observed sea-ice concentrations are fairly close to the suggested value of 90% in Lichey and Hellmer (2001). The length scale over which coherent motion has been observed justifies the use of sea-ice concentration fields from satellite or "global models" as these can usually be obtained at a spatial resolution of 100km (and often less). At the same time, there is no evidence to suggest that Schodlok et al. (2005)'s and Lichey and Hellmer (2001)'s results, which were, in both cases, derived for the Weddell sea

only, apply to other regions around the Antarctic continent, which have different ice conditions (see figures A–5 and A–6). In fact, the authors themselves point out that such factors as mean sea-ice thickness and/or ice viscosity, which vary from one region and/or type of ice to another, most probably influence the sea-ice concentration thresholds needed for joint iceberg sea-ice motion. Thus, we prefer to let go of the "greater than 90%" category in Lichey and Hellmer's formulation of sea-ice drag until the mechanisms behind the locking of iceberg and sea-ice are better understood. This omission is also motivated by the fact that it is unclear, and most probably untrue, that a "block" of iceberg(s) and sea-ice will move at a velocity that is purely that of sea-ice. We are not aware of any model or observational data on momentum exchange and feedback between iceberg and sea-ice. However, we expect the motion of the block to be influenced by sail/keel effects associated with the iceberg(s), with the magnitude and impact of these effects moreover dependent on the nature of air/water flow in a given region.

Roll-over criterion Weeks and Mellor (1978) have estimated that a tabular iceberg with a thickness between 130 and 260m and a density profile increasing with depth, will become unstable and roll-over if

$$\frac{D}{h} \quad < \quad \frac{0.09h + 58.32}{|D - 0.97h|}. \tag{2.14}$$

As a first approximation, we apply this roll-over criterion to all modeled icebergs irrespective of their sizes. When an iceberg rolls over, the diameter and thickness of the model iceberg are interchanged. This introduces small inconsistency in the

iceberg mass evolution because of the cylindrical shape of the iceberg and the increasing density profile assumed in the model, which is not rotated when the iceberg rolls over. The frequency of roll-over in our model remains to be investigated in detail. Note however that no roll-over has been observed in our simulations of giant icebergs.

Coastal collision. Observations show that icebergs colliding with the coast sometimes re-float off-shore under favorable environmental conditions (Bigg et al., 1997; Gustajtis and Buckley, 1978). Thus, modeled icebergs that hit the coast are still considered in the simulation. They remain stationary against the coastline until they melt or are pushed away from the coast by winds and/or ocean currents. This approach is further extended to submerged "topography" – defined as a region where water is shallower than the iceberg draft – so that an iceberg that hits marine "topography" will melt locally, until a change in forcing will push the iceberg away from the blocking topography, or until the iceberg draft becomes shallow enough for the berg to float across the topography.

2.3 Thermodynamics

Of all the processes believed to be important in iceberg deterioration, only a handful are understood well enough for quantitative estimates/parametrizations to exist. These include: (1) surface melting due to solar radiation, (2) melting due to buoyant vertical convection along the submerged portion of the iceberg, (3) melting due to forced convection of both exposed (air) and submerged (water) portions of the iceberg and (4) waterline wave erosion and subsequent calving of overhanging iceberg slabs (Job, 1978; El-Tahan et al., 1987; Savage, 2002). Here we omit both

solar radiation and forced wind convection processes as their contribution to iceberg melt is negligible (*e.g.,* see El-Tahan et al., 1987; Hanson, 1988; Savage, 2002). The parametrization of the individual melt processes included in our thermodynamics scheme are described below.

Wave erosion, M_{we}. Sustained wave action at the iceberg waterline can rapidly erode a rounded notch in the iceberg surface. As the notch deepens, an overhanging slab of ice is formed which will eventually break off (calve) due to increasing bending stresses in the slab. Following White et al. (1980), the wave erosion melt rate (m s^{-1}) is written:

$$M_{we} = 0.000146 \left(\frac{R}{H}\right)^{0.2} \left(\frac{H}{\tau_w}\right) (T_w - T_{ice}) \tag{2.15}$$

where R is the ice roughness height (0.01m); H and τ_w are the wave height and period respectively, T_w is the ambient water temperature (in this case, the surface water temperature) and T_{ice} is the temperature at the iceberg surface (-1.8℃). White et al. (1980) have also proposed a parametrization for the critical failure length of an overhanging slab, which can be used to estimate the calving time of a slab of given thickness and length. However, because observations show that calving intervals are on the order of 100 hours for water temperature close to 0℃ and as small as 10 hours for waters around 10℃ (Kubat et al., 2007; Ballicater Consulting Ltd., 2005), wave erosion and calving of overhanging slabs can be viewed as roughly instantaneous on time-scales of years. Thus, in our model, we assume that the overhanging slabs break off at the rate of wave erosion.

Calving can also occur underwater. The protruding slabs of ice break off due to buoyancy upthrust (ice is lighter than sea water) (Job, 1978; El-Tahan et al., 1987; Savage, 2002). The rate of creation and calving of underwater shelves has not been quantified. However, anecdotal observations of the submerged portions of tabular icebergs indicate that the underwater width of tabular icebergs is often smaller or on the order of the bergs' waterline length (Kristensen et al., 1982; Oceans Ltd., 2004). This suggests that underwater calving occurs at a similar or faster rate than the rate of calving of above-water overhanging slabs. Therefore, as a first order approximation, we take the melt rate of equation 2.15 to describe the combined effects of both underwater and above-water calving of protruding slabs of ice. A similar assumption is implicit in the models of Bigg et al. (1997) and Gladstone et al. (2001); the wave erosion melt rate is applied to the waterline length of a model berg that remains tabular throughout the simulation.

Because no wave data is available in the datasets used to force our IDM, we approximate the wave period and height in 2.15 using simple wind-wave prediction equations described by Goda (2003). These empirical equations relate wave parameters to wind speed under the condition that the surface winds blow for a sufficiently long period over some fetch length F. We take the fetch length to be 500×10^3m (500 km), which corresponds to the radius of a typical extra-tropical cyclone (*e.g.,* see Nielsen and Dole, 1992). Note that the dependence of wave height on fetch length saturates at roughly 1000km for windspeeds on the order of 10 m s^{-1}. Wave (height) build-up is also a function of time. The minimum time t_{min} (in hours) for full build-up is given by $t_{min} = \left(\frac{F}{1000}\right)^{0.73} U^{-0.46}$, where U is the wind speed (m s^{-1}) and F is

in meters. However, for simplicity this time dependency is ignored. Thus, the wave period is given by:

$$\tau_w = 3.3(H)^{0.63} \tag{2.16}$$

and the wave height, by:

$$H = \frac{0.3|\mathbf{u_a}|^2}{g}\left(1 - \left[1 + \frac{0.004\sqrt{gF}}{|\mathbf{u_a}|}\right]^{-2}\right) \tag{2.17}$$

where F is the fetch length of the wind.

Finally, note that, following Gladstone et al. (2001), we scale the wave erosion melt rate in Eqn. 2.15 by $\frac{1}{2}\left[1 + \cos(\frac{C^3}{\pi})\right]$, where C is the sea-ice concentration (%), to account for sea-ice damping of surface waves.

Forced convection, M_{fc}. Forced convection, also known as turbulent or basal convection, is most important at the base of the iceberg, where the differential velocity between the iceberg and the ocean sets up a turbulent heat transfer from water to berg. Weeks and Campbell (1973) used the general equation of forced convection for flow past a flat plate to derive an equation for the basal convective melt rate (m s^{-1}) of tabular icebergs. Rearranging slightly the equation of Weeks and Campbell (1973), we get

$$M_{fc} = 0.0058\left(\frac{Pr^{0.4}k}{L_f\nu^{0.8}\overline{\rho_i}}\right)\left(\frac{|\mathbf{u_w^n} - \mathbf{u_i}|^{0.8}}{D^{0.2}}\right)(T_w - T_{ice}) \tag{2.18}$$

where Pr, k and ν are the Prandtl number, the thermal conductivity and the kinematic viscosity of sea-water respectively and L_f is the latent heat of fusion of ice. For simplicity, we assume Pr, k and ν to be constant, and take the values corresponding

to sea water at 0℃ (see table 2–2). In 2.18, T_w is the ambient water temperature *i.e.,* , in this case, the water temperature at the base of the iceberg.

Buoyant convection, M_{bc}. The temperature and salinity difference between iceberg meltwater and surrounding sea water will act to set up a buoyancy-driven circulation along the submerged sides of the iceberg. The resulting buoyant convective heat transfer has been estimated by Neshyba and Josberger (1980) using a combination of theoretical considerations and laboratory measurement. The empirical relation for average buoyant melt rate (m s^{-1}) along the submerged sides of an iceberg of draft h_d is thus

$$M_{bc} = \frac{1}{h_d}\int_0^{h_d} 1.16 \times 10^{-2}(T_w(z) - T_{ice})z^{-1.4}dz \tag{2.19}$$

where z is the vertical coordinate and $T_w(z)$ is the ambient water temperature. Integrating 2.19 over n discrete ocean layers, one gets

$$M_{bc} = \frac{1.55 \times 10^{-2}}{h_d}\sum_{k=1}^{n}(T_k - T_{ice})^{1.6}h_k^{0.75} \tag{2.20}$$

where T_k is the average water temperature in the kth ocean layer and where h_k is the iceberg thickness ("height") in the same layer.

Implementation in the model. In the model, the wave erosion and the buoyant convection melt rates act to reduce the berg *diameter* while the forced convection (on the ice underside) reduces the iceberg *thickness*. Because melt due to wave erosion and buoyant convection is assumed to occur on all sides of the iceberg, the diameter is reduced by twice the melt rate given by the wave erosion (2.15) and buoyant convection (2.20) equations. In Bigg et al. (1997) and Gladstone et al.

(2001), the total side melt for fixed with-length ratio tabular icebergs was computed for the shorter iceberg side. It was then adjusted proportionally for the longer iceberg side, in order to keep the width-length ratio of the model iceberg constant (G. Bigg, 17 May 2007, pers. comm.).

2.4 Forcing Data

The fields required to force both the dynamics and thermodynamics schemes of the IDM are: (1) the ocean currents and temperatures, (2) the surface winds and (3) the sea-ice concentrations, thicknesses and velocities.

Ocean temperature and current, and sea-ice concentration fields are taken from the CCSM3.0 (Community Climate System Model V3.0) POP (Parallel Ocean Program) high-resolution hindcast experiment (gx1v3.210). The ocean and sea-ice datasets are freely available for the 1953-2000 period on the Earth Grid System website (see www.earthsystemgrid.org). Surface wind fields are taken from the CORE (Coordinated Ocean Reference Experiments) CIAF (Corrected Inter-Annual Forcing 1.0) datasets (based on the NCEP/NCAR reanalysis), which are also the atmospheric datasets used to force the CCSM3.0 POP hindcast run gx1v3.210. This wind data is freely available for 1953-2000 on the Geophysical Fluid Dynamics Laboratory (GFDL) website (see www.gfdl.noaa.gov).

In the region of interest, the CCSM3.0 POP fields have a horizontal resolution of 1.125° (∼65 km) longitude × ∼0.534° (∼60 km) latitude, with 40 discrete vertical levels, ranging in thickness from ∼10 meters (top 4 layers) to ∼250 meters (last 15 layers). For the wind forcing (CIAF), the horizontal resolution is 1.875° (∼110 km) longitude × ∼1.904° (∼210 km) latitude. The temporal resolution of all CCSM3.0

POP fields is a month and it is 6 hours for CIAF fields. A bi-linear interpolation calculates the forcing at the iceberg location. A linear interpolation in time is applied to the monthly CCSM3.0 POP fields.

Sea-ice concentrations from SSM/I (Special Sensor Microwave Imager) data were read into the ocean model and used to weight the atmosphere-ocean momentum and heat fluxes (S. Yeager, February 2007, pers. comm.). To force our iceberg model, we use the SSM/I sea-ice fraction fields interpolated onto the ocean model grid. In order to calculate sea-ice drag, we set sea-ice thickness to 1m everywhere and approximate the sea-ice velocity by that of surface water currents. The impact of this admittedly crude approximation is minimal in most regions as the sea-ice drag is generally 2 orders of magnitude smaller than the other forces governing iceberg drift (Gladstone et al., 2001). However, it can affect model accuracy in regions where sea-ice concentration is close to 100%.

2.5 Numerical Solution

The iceberg momentum equation 2.8 is solved using a high-accuracy fifth-order Cash-Karp Runge-Kutta method (see Press et al., 1992, for a detailed description of the algorithm). The time-step is calculated using an equation derived from a Von Neuman stability analysis of an iceberg momentum equation where only the water drag force was considered:

$$\Delta t \;=\; \frac{2M}{\rho_w c_w \sum_{k=1}^{n} A_k + \rho_w c_{dw} A_{hw}} = \frac{2M}{\rho_w (c_w DT + c_{dw} \pi R^2)} \tag{2.21}$$

where Δt [s] is the time-step. The time-step of Eqn. 2.21 is further reduced by a factor proportional to wind speed when the wind speed exceed 5m/s to take into account

the impact of the wind drag on numerical stability. Finally, we cap the maximum time-step at 600 seconds (ten minutes).To ensure computational efficiency, we also force the dynamic time-step to be at least 60 seconds (1 minute). If, for a given iceberg, a time-step of less than one minute is required for stability, the iceberg is artificially removed from the simulation. In our simulations, the implementation of this time-step calculation leads to an improvement of the model's numerical stability; less than 5% of model iceberg in a given run become unstable. Numerical instability is a documented, and as of yet unsolved, problem in iceberg drift models. Indeed, even the operational model of the International Ice Patrol (IIP)"sometimes becomes unstable"(Savage, 2002). Recently, Kubat et al. (2005) have worked on developing a new, and more stable, operational model for the Canadian Ice Service (CIS). In the improved model, Kubat et al. (2005) have opted for an implicit Euler numerical scheme. By definition, a fully implicit numerical scheme is unconditionally stable. However, while longer time-steps are still stable, they result in a decreased model precision.

The melt routine is invoked once every six hours and the melt terms are computed under the assumption that current water, wind and ocean conditions are constant over the six hours. This is a valid assumption given that we expect the melting process of an iceberg to be the result of sustained forcing rather than of sort-lived variations in wind, ocean currents and sea-ice.

CHAPTER 3
Results

3.1 Climatology of large-scale Antarctic iceberg drift

Results from a large-scale IDM simulation of Antarctic icebergs for the period 1979-2000 are presented in this section. The model has been run with icebergs discharged at 182 locations around the Antarctic continent (see figure 3–1). Jacka and Giles (2007) estimate the half-life of typical iceberg (up to 3200m in length) to be on the order of two hundred days (7 months) in the open ocean[1] . For this reason and for clarity of the spaghetti plots, we seed the model every second year starting from January 1979 until January 1995 (for a total of 9 launch dates). The last simulation is launched in 1995 to allow most of the model icebergs to melt away by the end of simulation in 2000. At each seeding location, five icebergs of different sizes (see table 3–1) were released at each launch date, for a total of 8190 icebergs over the 1979-2000 period. The choice of iceberg sizes is consistent with the range of dimension observed in the coastal regions of Antarctica (*e.g.,* see Orheim, 1980; Vinje, 1980; Tchernia and Jeannin, 1984; Jacobs et al., 1992; Gladstone et al., 2001; Jacka and Giles, 2007). Giant icebergs are however omitted from the simulations. Giant iceberg calving is episodic and infrequent. Moreover, the giant icebergs melt much

[1] However, the authors also point out that this estimate might "not be applicable to coastal icebergs in cold slow-moving water"(Jacka and Giles, 2007).

more slowly, and drift much further than normal-sized icebergs. Thus, a systematic seeding of giant icebergs in the simulation would results in biases in the extent and distribution of modeled trajectories.

A spaghetti plot of all the modeled trajectories is shown in figure 3–2. Note that the general picture of modeled icebergs in figure 3–2 is partially masked by the year-to-year variability in individual iceberg trajectories. The details of modeled iceberg movement can be seen more clearly in spaghetti plots of 910 (182 launch sites, 5 sizes) icebergs launched in individual years shown in fig. 3–3 for 1979,1981,1987 and 1989. Nevertheless, apparent in figure 3–2 (and also in figure 3–3) are the three main modes of motion of Antarctic icebergs as inferred from satellite, radar and ship observations of Antarctic icebergs (*e.g.,* see Tchernia and Jeannin, 1984; Vinje, 1980; Orheim, 1980; Keys and Fowler, 1989; Gladstone and Bigg, 2002) as well as a previous large-scale simulations of Antarctic iceberg behavior (Gladstone et al., 2001): (1) westward drift of icebergs near the coast, in the Antarctic Coastal Current, (2) localized northward motion of icebergs away from the coast at retroflection points, and (3) eastward drift of icebergs in the open ocean, in the Antarctic Circumpolar Current (ACC).

In the model, all icebergs that leave the coast have similar trajectories characterized by a sharp curvature of the berg path from its initial westward drift to its final eastward drift. A similar behavior has been observed in satellite-tracked icebergs by Tchernia and Jeannin (1984) (see figure 3–4), who refer to this type of motion as "retroflection". Model results show that retroflection tends to occur in the same fairly narrow regions from one year to another. In fact, the motion of icebergs away

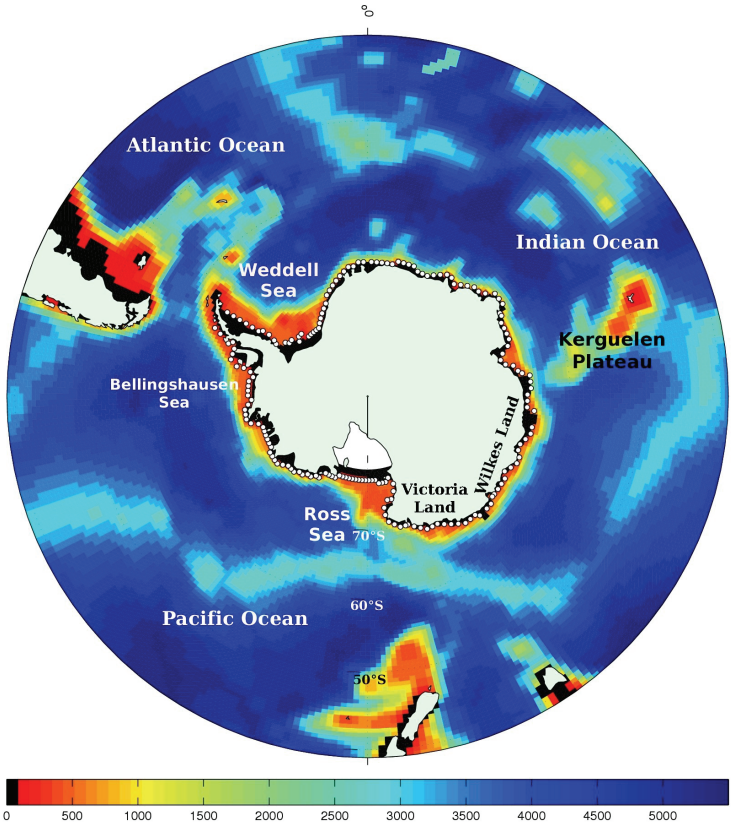

Figure 3–1: The 182 iceberg launch sites (white circles) used in the 1979-2000 climatology model run. Also shown is the Parallel Ocean Program (POP) model domain and bathymetry (m). The black and white regions correspond to land and ice shelves in the POP model respectively. In the figure, both regions are partially masked by the true continents in very light green.

Table 3–1: Iceberg size distribution used in the climatology run

Size Class	Berg Diameter (m)	Berg Thickness (m)	Freeboard (m) (% of thickness)	Mass (kg)
1	150	100	24 (24%)	1.37×10^9
2	300	150	30 (20%)	8.69×10^9
3	800	250	42 (17%)	1.07×10^{11}
4	1500	300	48 (16%)	4.57×10^{11}
5	2100	350	54 (15%)	1.05×10^{12}

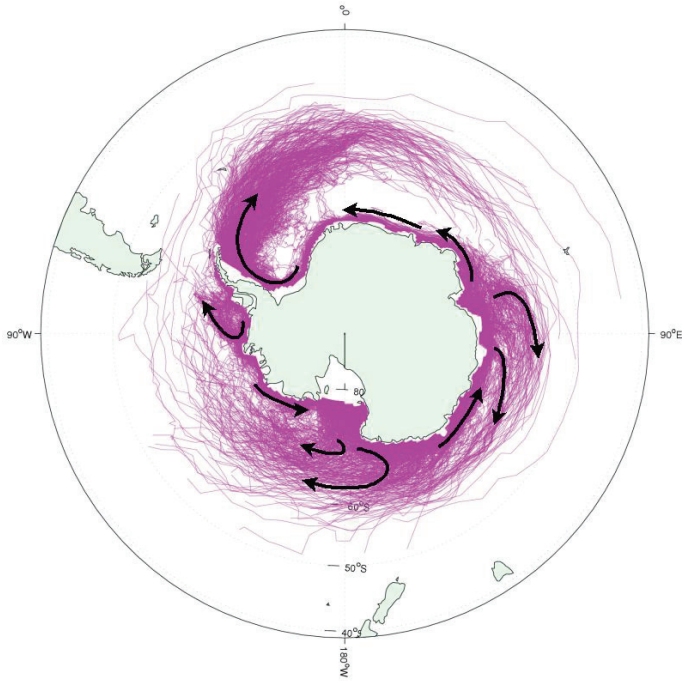

Figure 3–2: 1979-2000 climatology of simulated iceberg trajectories in the Southern Ocean. Arrows indicate direction.

from the coast is localized in five main regions: (1) in the Weddell Sea and along the Antarctic Peninsula (∼50-60°W), (2) over the Kerguelen Plateau (∼70-80°E), (3) off Victoria Land (around 150°E), (4) in the Ross Sea (∼170-180°W) and, (5) in the Bellingshausen Sea (∼80-90°W).

Iceberg retroflection in the Weddell and Ross seas can be explained by the presence of strong cyclonic (clockwise) ocean gyres and climatological atmospheric low pressure systems in both seas, and the presence of relatively strong northward Katabatic winds (see Appendix A for climatology of forcing fields of the IDM). More specifically, the four main (1-4) regions of northward motion occur near underwater topography, most notably the Kerguelen Plateau (see figure 3–1), indicating that

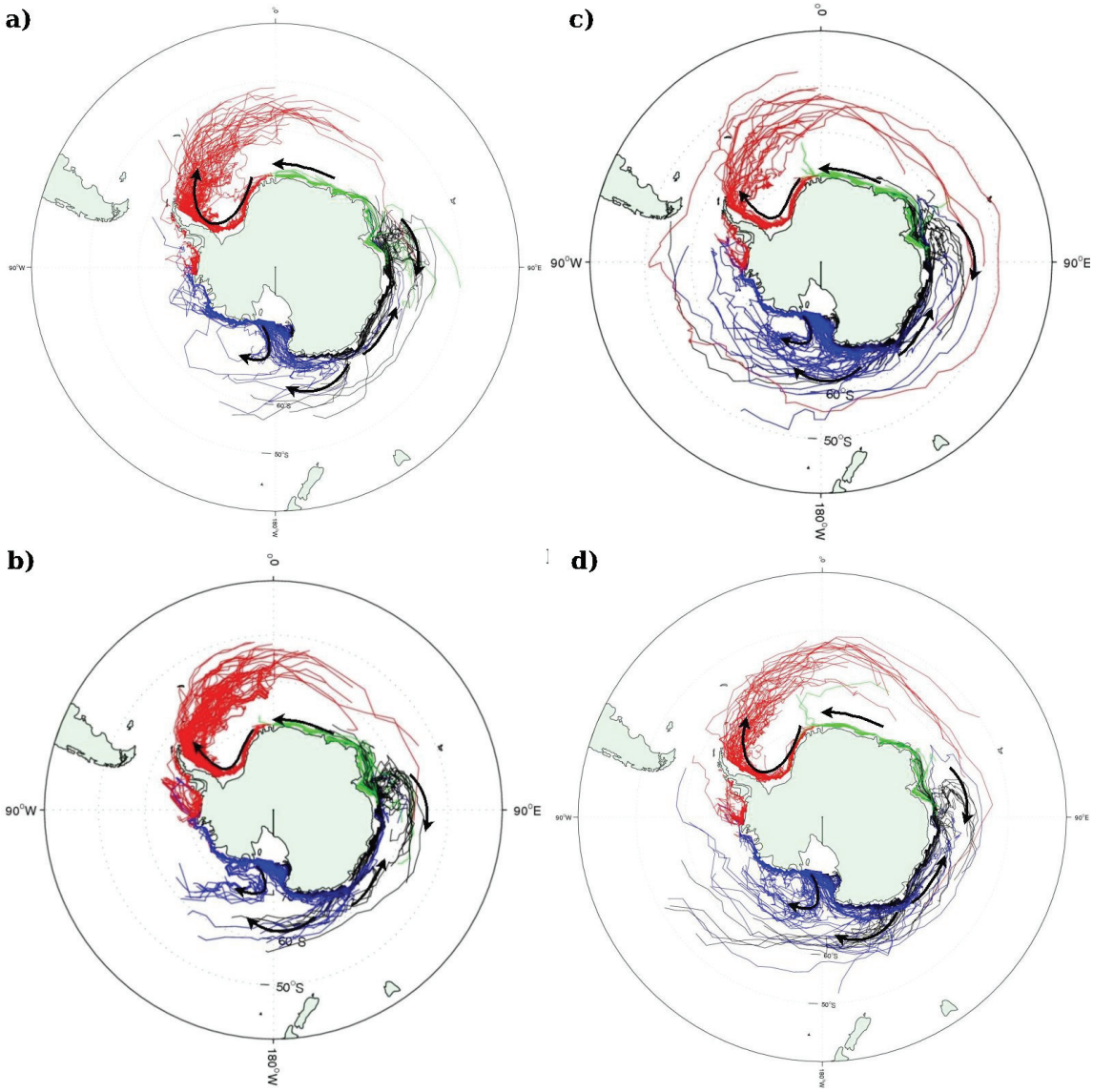

Figure 3–3: Eleven-year runs of five iceberg size classes launched at 182 sites around Antarctica in January of 1979(a), 1981(b),1987(c) and 1989(d) respectively. Trajectories are color-coded according to start (launch) position; green for 0-90°E, black for 90-180°E, blue for 180-90°W and red for 90-0°W.

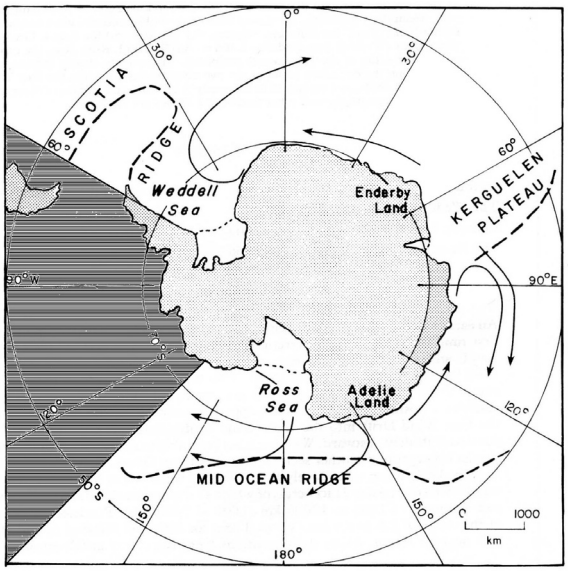

Figure 3–4: Main trends of movement as shown by 21 satellite-tracked icebergs during the 1972-1983 period. Starting positions of tracked icebergs were between 47°E and 137°W. The stripped area indicates the region were icebergs were not tracked.(Figure adapted from Tchernia and Jeannin, 1984, , Reprinted with the permission of Polar Record.)

topographic steering of ocean currents plays a role in the northward iceberg motion observed in these regions (Tchernia and Jeannin, 1984; Keys and Fowler, 1989; Gladstone et al., 2001). An examination of ocean forcing fields show the occasional appearance of a small elongated recirculation in ocean currents (as simulated in the POP ocean model) in the Bellingshausen Sea (see figure 3–5), which might explain the non-negligible detrainment of icebergs in the later region.

The modeled behavior is in agreement with observations by Tchernia and Jeannin (1984) who have examined the motion of 21 satellite-tracked icebergs between 1972-1983 around four-fifths of the Antarctic periphery (no icebergs were tracked in the Bellingshausen and Amundsen seas because of the lack of infrastructure/ships

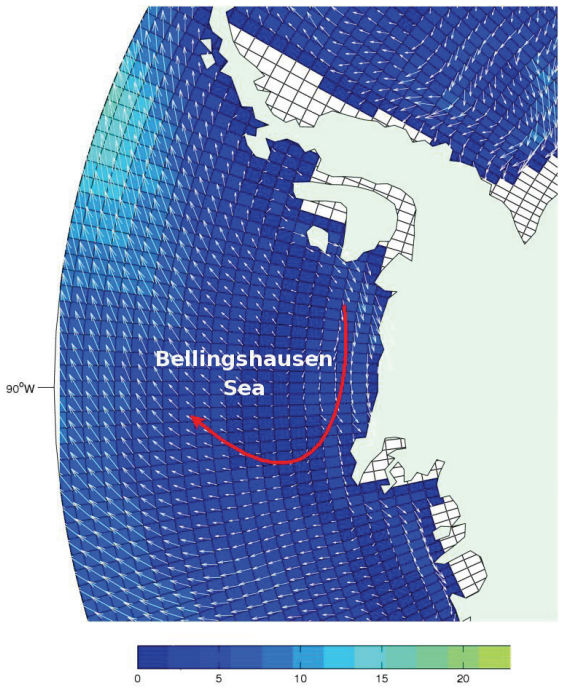

Figure 3–5: POP ocean currents in the Bellingshausen Sea for November 1996. Shown is the speed (cm s^{-1}) and direction (white arrows) of the currents. The red arrow roughly indicates the Bellingshausen sea recirculation.

necessary to tag the icebergs in these regions). Note also that the authors only examined the drift of icebergs with starting position between 47°E and 137°W. For this reason modeled retroflection zones (1) and (5) – listed above – are not shown in figure 3–4. Of the four retroflection zones resolved in Tchernia and Jeannin (1984)'s dataset, three are well reproduced by the model, mainly: (1) over the Kerguelen Plateau, (2) off Adelie Land and (3) in the Ross sea. The fourth observed retroflection zone, near 30°W (on the eastern side of the Weddell sea), is further west in the simulation near 10°W and only a negligible portion of the modeled icebergs retroflect in the later area.

Good agreement between model and observations in other regions around Antarctica suggests that the divergence between data and simulation between 10-30°W is due to inaccuracies in the forcing fields rather than in the formulation of the physics of the model itself. Amongst other, the Katabatic winds blowing offshore the continent are not well resolved in the NCEP-derived wind fields (with horizontal resolution of 1.9°) used to force our IDM; the winds weaken too fast as one moves northward and away from the coast. Observations and high-resolution model simulation of Antarctic Katabatic winds (*e.g.,* see Parish and Bromwich, 1998; van de Broeke et al., 1997) suggest that the winds should extend northward much further than is seen in the NCEP forcing fields and, specifically, should have speeds of 6-9m s^{-1} up to 65°S, rather than of 1-2m s^{-1} as is seen in our wind forcing fields. Moreover, Tchernia and Jeannin (1984) mention the appearance of meanders and eddies in the trajectories of two of the three tracked icebergs shortly before they retroflected near 30°W, indicating that finer scale forcing, such as the passage of mesoscale weather systems and oceanic eddies, which are not resolved in the monthly-mean ocean forcing of the IDM, might play a role in iceberg detrainment from the coast in the region.

Additionally, there is some indication that the climate of the Southern Ocean has been slowly changing since the 1960s, associated with a gradual shift of the Southern Annular Mode (SAM) towards a more positive phase (*e.g.,* see Marshall, 2003). The SAM is the most important pattern of month-to-month and year-to-year climate variability in the middle and high latitudes of the southern hemisphere. The positive phase of SAM is characterized by a southward meridional shift of westerly winds resulting in enhanced westerlies over the Southern Ocean and substantial changes in

(surface) ocean currents and temperatures amongst other (Marshall, 2003; Lovenduski and Gruber, 2005; Gupta and England, 2006). It is unclear if these changes have affected the broad patterns of iceberg motion over time. We can only speculate that the changes in retroflection zones *not* associated with topographic steering (such as the one just discussed) might have been influenced by the recent changes in the Southern Ocean environment.

As for the simulated retroreflection zone (1), anecdotal observations of small and medium icebergs (diameter on the order of 10^2-10^3m) suggest that the northward motion of icebergs in the Weddell Sea is common (Gladstone and Bigg, 2002). The northward motion of icebergs parallel to the Antarctic peninsula (on its eastward flank) is also evident in the distribution of the reported positions of giant icebergs tracked by satellite during the 1978-2001 period (see figure 3–6). Because of their size, the giant icebergs are expected to drift differently from smaller iceberg due to, amongst other, the relative increase in importance of the Coriolis force, which is proportional to the mass of the berg. Nonetheless, the drift of giant icebergs offers a reasonable approximation of the movement of smaller bergs. Indeed, figure 3–6 shows that, similarly to medium and small icebergs, giant icebergs have a tendency to retroflect in specific zones located over the Kerguelen Plateau, in the Ross Sea and in the Weddell Sea. The number of iceberg sightings along the eastern side of the Antarctic Peninsula lends credibility to the modeled detrainment of icebergs in the same region. In figure 3–7, we compare the northernmost limit of the modeled trajectories with known limits of ship-based iceberg sightings. There are uncertainties in both datasets. On one hand, the observed iceberg limit is in fact a compilation

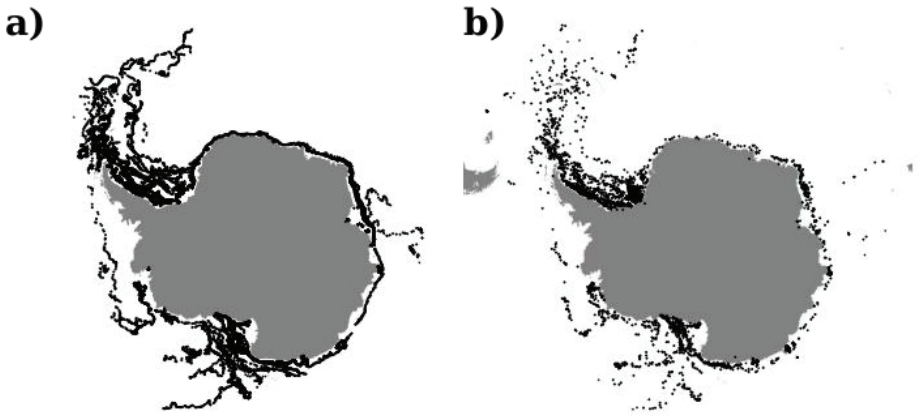

Figure 3–6: All positions reported for all Southern Ocean giant icebergs tracked by (a) Brigham Young University (BYU) (1978, 1992-2001) and (b) the National Ice Center (1978-2001) (Images courtesy of David Young at BYU [http://www.scp.byu.edu/data/iceberg/database1.html]).

of ship-based sighting during the navigation season (1947-1962) *i.e.,* one expects the dataset to be biased because of relative over-sighting of icebergs in shipping lanes when compared with areas where ships rarely travel. On the other hand, the modeled iceberg distribution is based on an arbitrary calving flux, which may have resulted in an artificial increase/decrease of icebergs in certain regions. Nonetheless, we take the good agreement between the observed and modeled northern extent of iceberg as a positive validation of our IDM

Finally, let us note that the collocation of the main surface ocean currents and iceberg drift features, one could conclude that iceberg are passive tracers advected by the (surface) oceanic currents. However, a simulation of passive tracers, released in the same location as the icebergs in the climatology runs, shows a drastically different behavior (see figure 3–8). In fact, a few tracers are advected from the Weddell Sea

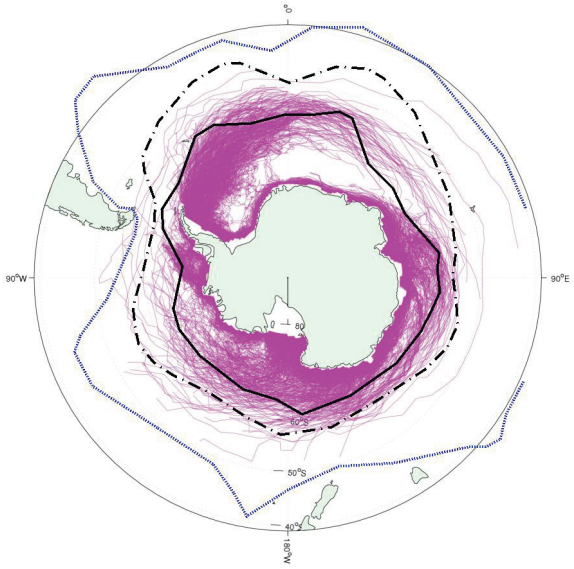

Figure 3–7: Observed (from Soviet Antarctic Survey (1966)) northernmost iceberg limits for the December-March period from the 18th century to 1966 (blue dotted line), for the 1947-1962 navigation season (black dash-dotted line) overlaid over the modeled climatology (1979-2001) of Southern Ocean iceberg trajectories. The continuous black line indicate the region past which iceberg sightings become rare *i.e.,* sightings at intervals of more than 70 km, based on the 1947-1962 navigation season(Soviet Antarctic Survey, 1966)

by the relatively strong eastward branch of the Weddell gyre. However, a closer inspection of model results reveals that most of the tracers that do break away from the coast have been launched a few tens of degrees further from the coastline than the tracers that collide with the continent from the start of the simulation. The behavior of the modeled tracers can be explained by the fact that immediately adjacent to the coast, the currents tend to have a non-negligible southward component (Ekman drift) in their direction, which will continuously push the tracers towards the coast. In the case of model icebergs, the southward motion imposed by the surface currents

is partially opposed by (1) the winds blowing offshore the continent and (2) the sea surface tilt force.

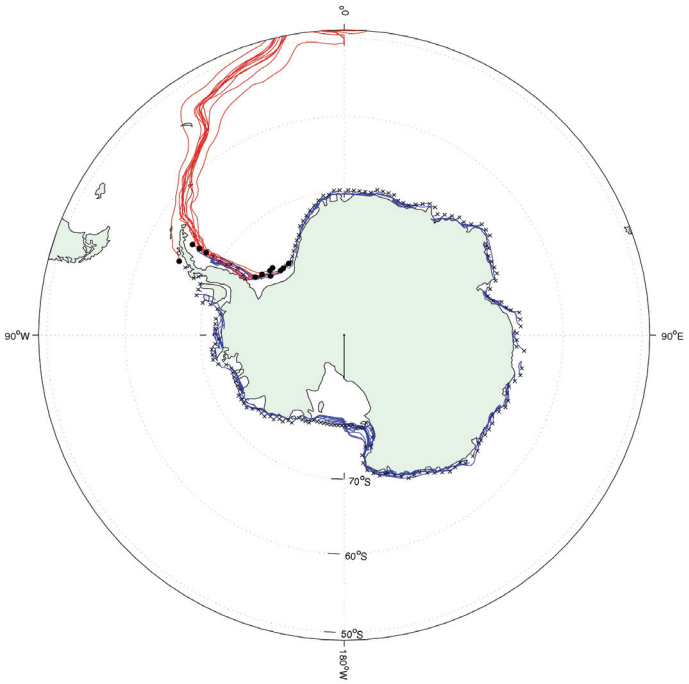

Figure 3–8: Same as figure 3–3(a), but with passive tracers advected by surface ocean currents instead of icebergs modeled using the full IDM. Trajectories that break off the coast are colored red, and their initial position marked with a black circle. All other trajectories in blue, with an × at their initial position.

3.2 Hindcast of individual giant iceberg drift tracks

3.2.1 Iceberg Observation

The National Ice Center(NIC) maintains a public "giant iceberg" database on their Web site (see http://www.natice.noaa.gov/products/iceberg/). A giant iceberg, is defined by the NIC, as a berg with a horizontal long axis of at least 10 nautical miles *i.e.,* roughly 18.5 km (1.0nm ≈ 1.852 km). The database dates back to 1976 and is continuously updated. Presently (August 2007), it contains data on

124 icebergs (not counting icebergs resulting from the split off an iceberg into one or more pieces, which are also monitored). Each iceberg is identified by a name composed of the letter of the Antarctic quadrant in which it was originally sighted, along with a sequential number (*e.g.,* A10 for the 10th iceberg sighted in quadrant A); quadrant A corresponds to 0-90°W (Bellingshausen/Weddell Sea); quadrant B, to 90-180°W (Amundsen/Eastern Ross Sea) ; quadrant C, to 180-90°E (Western Ross Sea/Wilkes land) and quadrant D, to 90-0°E (Amery/Eastern Weddell Sea).

The NIC estimates the horizontal size (in nautical miles) and position (in latitude/longitude) of the tracked icebergs from various types of satellite imagery, including optical imagery, microwave radiometry, and synthetic aperture radar. This information is recorded in the datasets at irregular intervals ranging from 15-20 days to months. Each iceberg is tracked until it breaks up below the resolution of satellite imagery. Currently, the smallest recorded horizontal berg size in the dataset is 5×2 nautical miles .

In our study, we consider all NIC icebergs that satisfy three basic requirements. First, the icebergs must have been tracked during the 1979-2000 period, which corresponds to years covered by the ocean and wind forcing of our IDM. Second, we ignore grounded icebergs as well as icebergs which travel in regions mapped as land in the forcing field of our ocean model. And, third, we ignore iceberg records than contain less than 10 entries. More generally, we ignore all iceberg trajectories that, once plotted, show several outliers, which appear as severe discontinuities in the recorded iceberg position. Both Long et al. (2002) and Silva et al. (2006) have pointed out the existence of several errors in the iceberg position and size values recorded in

the NIC dataset. A group led by D. Long at Brigham Young University (BYU), have re-analyzed, at much higher resolution, the trajectory – but not the size – of a number of giant icebergs for the 1978, 1992-2001 period. Figure 3–9 show two examples of the high resolution of BYU trajectories, when compared to the ones recorded at NIC. The BYU reanalysis is also publicly available on their website

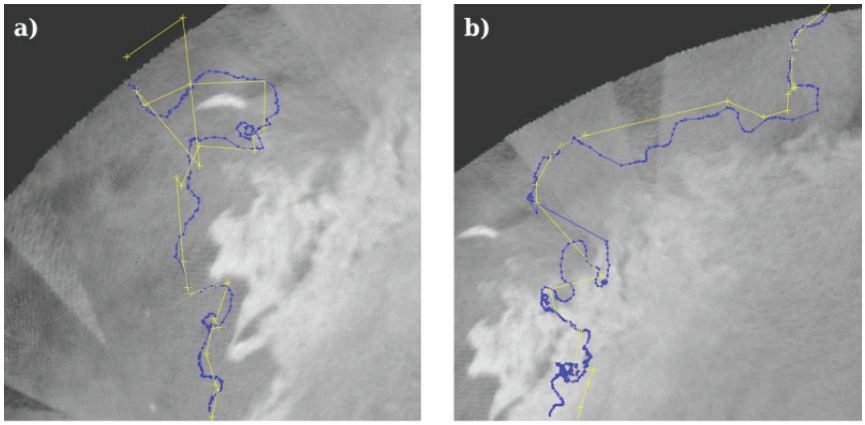

Figure 3–9: Comparison of the iceberg tracks as recorded by the National Ice Center (in yellow) and Brigham Young University (in blue) respectively for icebergs A22B (a) and A22C (b).(Images courtesy of David Young at BYU [http://www.scp.byu.edu/data/iceberg/database1.html]).

(see http://www.scp.byu.edu/data/iceberg/database1.html) however, to provide a larger set of data for the validation of our model and for consistency, we use the NIC trajectories. In this study, the obvious outliers in NIC trajectories are simply deleted. The more subtle errors in trajectory – (as seen in the final part of the trajectory of berg A22B in figure 3–9(a)) – and the potential size errors in the datasets are not addressed. The final database considered in our study consists of twenty-four iceberg satisfying the above criteria have been considered. However, a total of twenty nine NIC iceberg drift tracks were hindcasted, as the trajectory of some of the individual

icebergs was split into two or several segments modeled independently. This was done when the initial iceberg motion was not reproduced in the simulation, to verify if a later segment of the trajectory could be successfully simulated.

3.2.2 Numerical Procedure

The model icebergs were seeded at the date and position listed in the NIC datasets. The diameter of the model iceberg was chosen so that the horizontal area of the model iceberg matched that of the observed one *i.e.,* so that the equality $a \times b = \pi \left(\frac{D}{2}\right)^2$ is satisfied, where a and b are, respectively, the long and short axis of the observed iceberg, and D is the diameter of the modeled iceberg. Since the thickness data is not available in the NIC dataset, for each observed drift track, we launched five model icebergs with thicknesses of 100, 150, 200, 250 and 300 m respectively. Note that because the NIC size measurements are "coarse and infrequently updated"(Silva et al., 2006) and do not include thickness data, we do not attempt to calibrate the IDM thermodynamics against observations. Anecdotal observation suggest that, at time of calving, a typical (giant) iceberg will have a thickness in the 250-300 m range (*e.g.,* see Jacobs et al., 1992; Keys and Fowler, 1989; Gladstone et al., 2001; Lichey and Hellmer, 2001; Silva et al., 2006). We also consider thinner iceberg to account for possible iceberg melting prior to the start of the iceberg record and/or simulation such as in the case when only a segment of the total recorded trajectory is simulated.

IDM performance is evaluated based on the model's ability to reproduce the shape and timing of the observed track. When both the timing and shape of the icebergs are in relatively good agreement, model error is computed as in Kubat et al.

(2005) *i.e.,*

$$E = \frac{\Delta L_{om}}{L_o} \times 100 \tag{3.1}$$

where E is the model error in percent (%); ΔL_{om} (km) is the distance between model and observed endpoints, and L_o (km) is the length of the observed track. The model endpoint is taken to be the position of the simulated iceberg at the time where the real iceberg tracked ended. Because of the output interval of the model, the maximum time difference between model and observed endpoints is one week. For simplicity we take L_o to be the straight path distance between the initial and final position of the observed iceberg. Because in most cases, the real iceberg drift track is characterized by meanders along a straight path, our calculation of L_o results in a slight *overestimation* of the model error.

Simulations in which the shape but not the timing of the observed track was reproduced were also considered to be reasonably successful. This is because the goal of large-scale iceberg modeling is not so much to produce a timely forecast of iceberg motion but rather to create a climatology of the overall patterns of motion (and melt) of icebergs over an extended period of time. For modeled icebergs that reached the vicinity of the observed track endpoint, we calculate a time delay ϵ (in days) between the recorded and simulation end date such that

$$\epsilon = t_m - t_o \tag{3.2}$$

where t_m and the t_o are the end dates of the simulated and observed trajectories respectively and where ϵ is in days. A *positive* time delay indicates that the simulated

track reached the observed endpoint *after* the recorded time. No quantitative error was calculated for simulations where the general shape of the observed trajectory was not reproduced.

3.2.3 Overview of results

In figure 3–10 we show the twenty nine *observed* NIC iceberg tracks that were hindcasted. The distribution of hindcasted icebergs per quadrant follows that of the NIC dataset *i.e.,* most (12) of tracks are in quadrant A (0-90°W) (Bellingshausen/Weddell) with the remaining tracks split almost equally between the other quadrants. The shape and timing of twelve of the observed tracks (41%) is well simulated. In six cases (21%), the model reproduced the shape of the observed track, but the timing was off, and in eleven (38%) cases the simulations[2] showed no agreement with observation. Also shown in figure 3–10 is a measure of the ability of the model to hindcast the individual tracks. Well simulated tracks are primarily located near the southern tip of the Antarctic Peninsula and, more generally, in the open ocean. The problematic trajectories are concentrated in the southern portions of the Weddell and Ross seas, and along the Antarctic coastline although some trajectories were well simulated in this region with errors in the timing (see discussion for details on these errors).

[2] In this section, we use the term "simulation" to refer to the hindcast of a single observed iceberg, which, in each case, consists of *five* modeled trajectories corresponding to icebergs of initial thicknesses ranging from 100 to 300m. The simulation is considered successful if at least one of the modeled trajectories agrees with observations

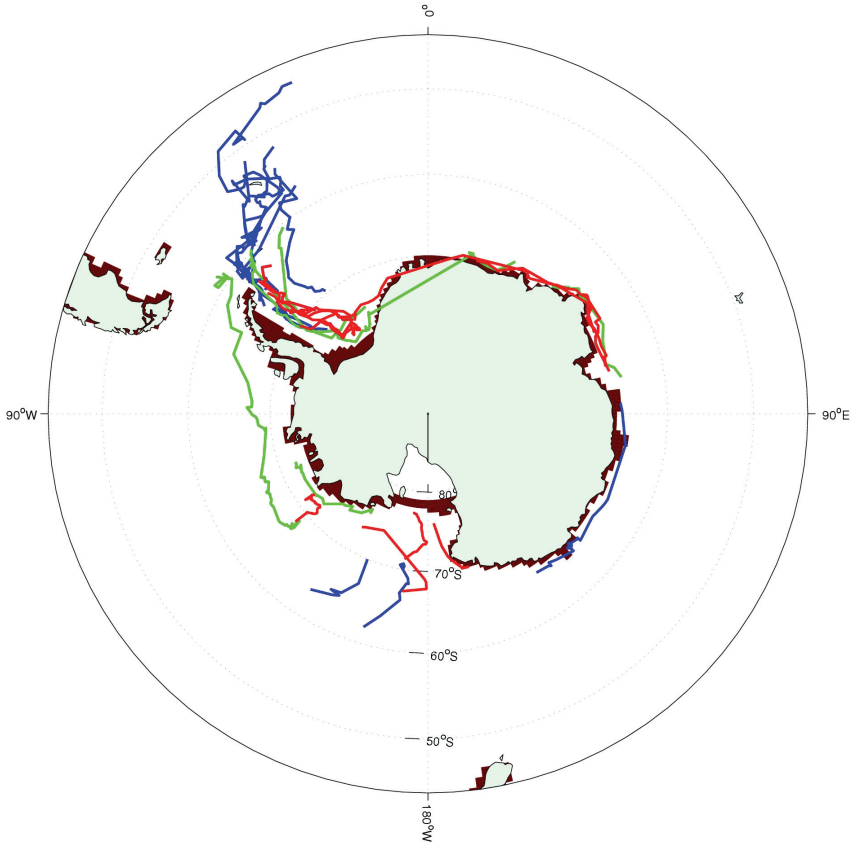

Figure 3–10: Location of the trajectories of the twenty-nine NIC iceberg hindcasted in this study. The iceberg tracks are color-coded according to the IDM's ability to simulate them: Blue: shape and timing is well simulated, Green: shape is well simulated but timing is off, and Red: not well simulated.

Detailed track information including the track number, duration and length L_o as well as the initial size, the NIC identification of the iceberg being modeled, and the model error (when appropriate) is provided in tables 3–2, 3–3, 3–4, 3–5, 3–6 and 3–7.

As a first test of the dependence of model performance on track duration and/or length, all simulations were given a number ranging from 0 to 1 according to the accuracy of the simulation. Simulations in which both the shape and the timing agreed reasonably well with observations were given a value of 1.0, simulations in which only the shape was successfully reproduced were given a value of 0.5 and bad simulations, a value of zero. The correlation (r_c) between the "accuracy value" and the length L_o was 0.23 and it was 0.12 between the accuracy value and the duration of the track. Both values are not significant at 95% confidence level. The corresponding coefficients of determinations (r_c^2) are 0.05 and 0.01 respectively, indicating that not more than 5% of the variation in model performance is explained by either track duration or length. Finally note that a weak positive correlation of 0.61 (significant at the 95% confidence level) was found between track duration and length indicating that there is only a weak tendency for longer (time-wise) tracks to be lengthier (spatially) in our dataset.

3.2.4 Simulations in which both shape and timing is reproduced

In twelve out of the twenty-nine simulations, both the shape and the timing of the observed trajectory were reproduced with reasonable accuracy. These successful hindcasts are shown in figures 3–11, 3–12, 3–13.

Table 3–2: Iceberg size and drift information for tracks # 1 to 4

Track #	NIC ID	Start Yr/Day	Hor. dim. (nm)	Duration Yr/Day	L_o (km)	Error (E) Range
1	A20A	1986/253	45×30	1/200	2036	8-100%
2	A20B	1986/253	45×22	1/152	2942	10.5-99%
3	A22B	1999/77	35×12	1/76	1717	42-125%
4	A22C	1998/251	14×3	2/104	1781	32-158%

Table 3–3: Iceberg size and drift information for tracks # 5 to 8

Track #	NIC ID	Start Yr/Day	Hor. dim. (nm)	Duration Yr/Day	L_o (km)	Error (E) Range
5	A23B	1998/98	11×9	1/55	809	16-177%
6	A25	1989/32	25×7	1/59	1753	22-111%
7	A35A	2000/46	17×9	0/192	582	0.9-55%
8	A35B	2000/46	13×6	0/108	290	29-53%

Table 3–4: Iceberg size and drift information for tracks # 9 to 12

Track #	NIC ID	Start Yr/Day	Hor. dim. (nm)	Duration Yr/Day	L_o (km)	Error (E) Range
9	B02	1984/341	20×10	1/24	972	50-119%
10	B06	1997/25	20×15	1/70	884	21-127%
11	B09A	1991/27	30×19	7/235	2602	5-73%
12	D11	2000/151	30×8	0/204	1358	28-53%

Table 3–5: Iceberg size and drift information for tracks # 13 to 15

Track #	NIC ID	Start Yr/Day	Hor. dim. (nm)	Duration Yr/Day	L_o (km)	ϵ_{min} ; ϵ_{max} days (% of duration)
13	B01	1982/343	18×13	4/14	3578	2918(130%) ; 3187(216%)
14	B04	1984/166	18×4	0/225	1280	200(89%) ; 767(340%)
15	B06	1987/105	20×20	1/335	1269	1035(147%) ; 2428(346%)

Table 3–6: Iceberg size and drift information for tracks # 16 to 18

Track #	NIC ID	Start Yr/Day	Hor. dim. (nm)	Duration Yr/Day	L_o (km)	ϵ_{min} ; ϵ_{max} days (% of duration)
16	B10A	1997/343	42×21	2/261	3565	-415(-44%) ; -543(-55%)
17	C07	1988/79	20×10	0/312	1152	3933(1260%) ; 4164(1715%)
18	C07	1990/128	20×20	1/358	1715	1980(274%) ; 2687(372%)

Table 3–7: Iceberg size and drift information for tracks # 19 to 29

Track #	NIC ID	Start Yr/Day	Hor. dim. (nm)	Duration Yr/Day	L_o (km)
19	A22B	1997/266	38×19	1/252	1300
20	A23B	1997/206	11×9	1/312	1300
21	A35A	1998/277	17×12	1/34	534
22	A35B	1998/277	13×6	1/187	849
23	B07	1990/186	10×5	1/225	1051
24	B09	1989/19	76×19	0/197	657
25	B10A	1995/231	60×25	1/133	454
26	B15E	2000/236	23×6	0/109	778
27	C05	1994/221	29×18	1/85	1094
28	D11	1999/41	48×9	1/110	1394
29	D12	1997/5	28×22	1/181	1899

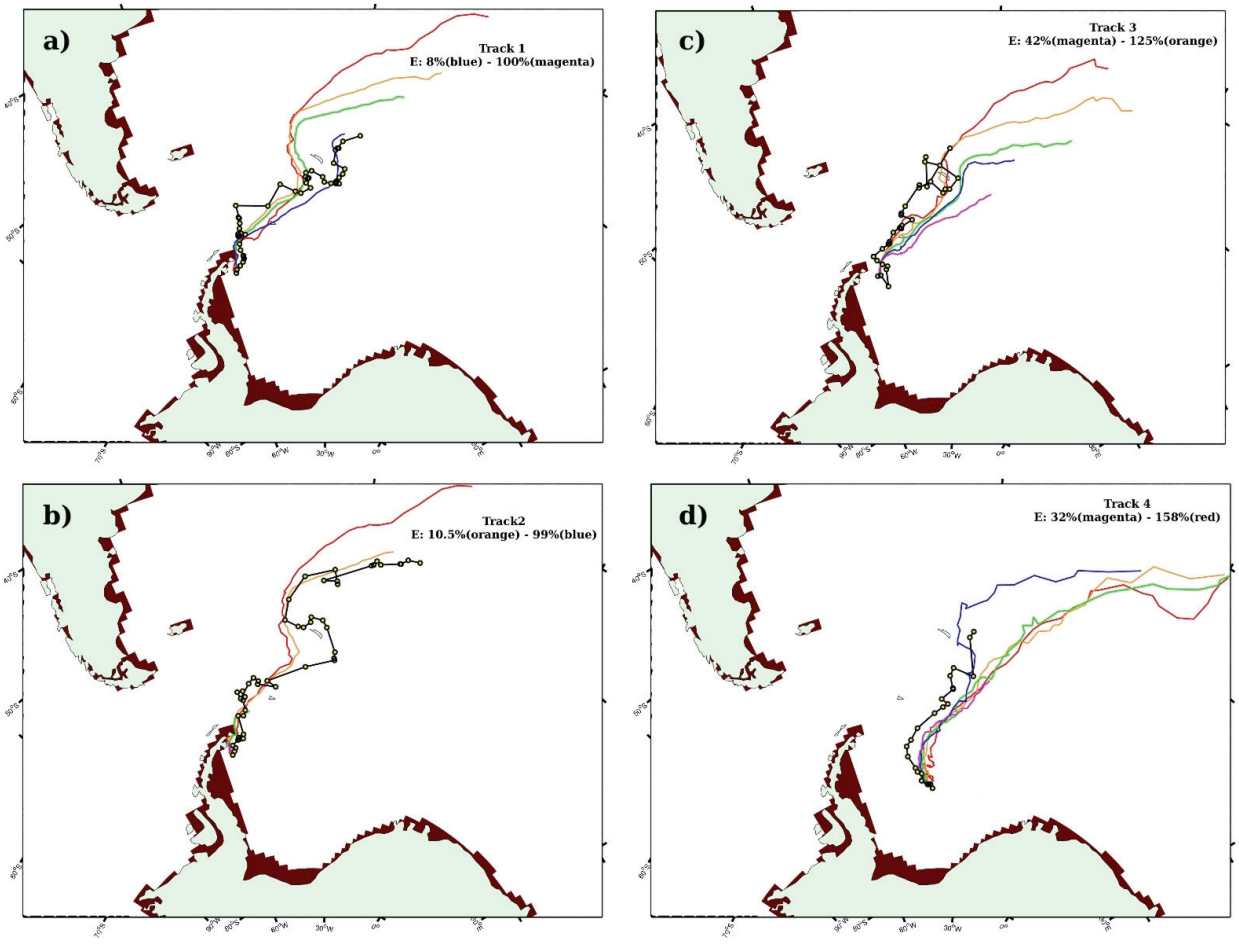

Figure 3–11: Predicted (colored lines) and observed (black lines) giant iceberg tracks 1 to 4 (a-d). The yellow circles indicate observations as recorded in the NIC giant-iceberg database. On each plot, we show the predicted trajectories for five different initial thicknesses: 100m(red), 150m(orange), 200m(green), 250(blue) and 300m(magenta). Detailed track information is shown in table 3–2.

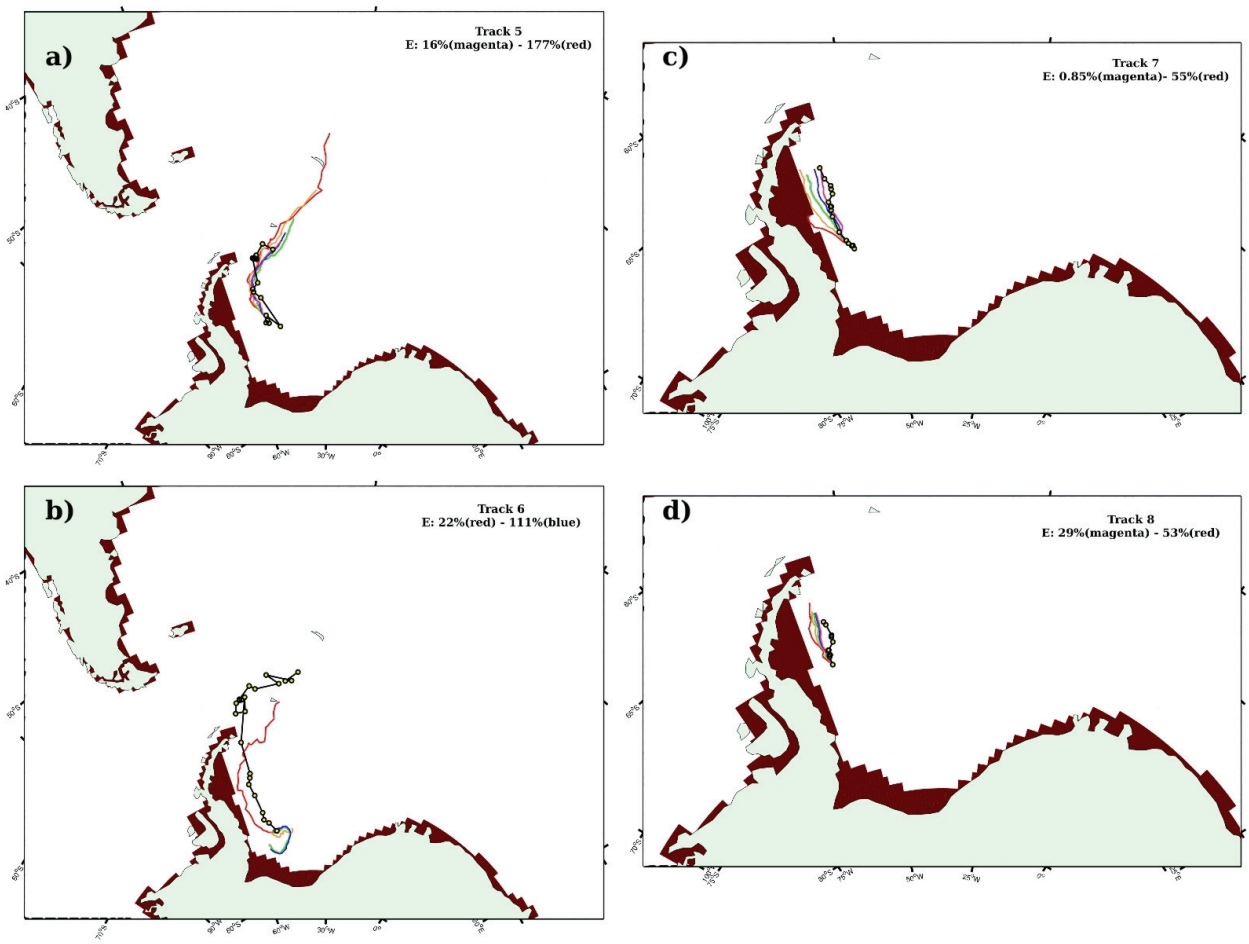

Figure 3–12: Same as figure 3–11 but for tracks 5 to 8 (a-d). Track information is shown in table 3–3.

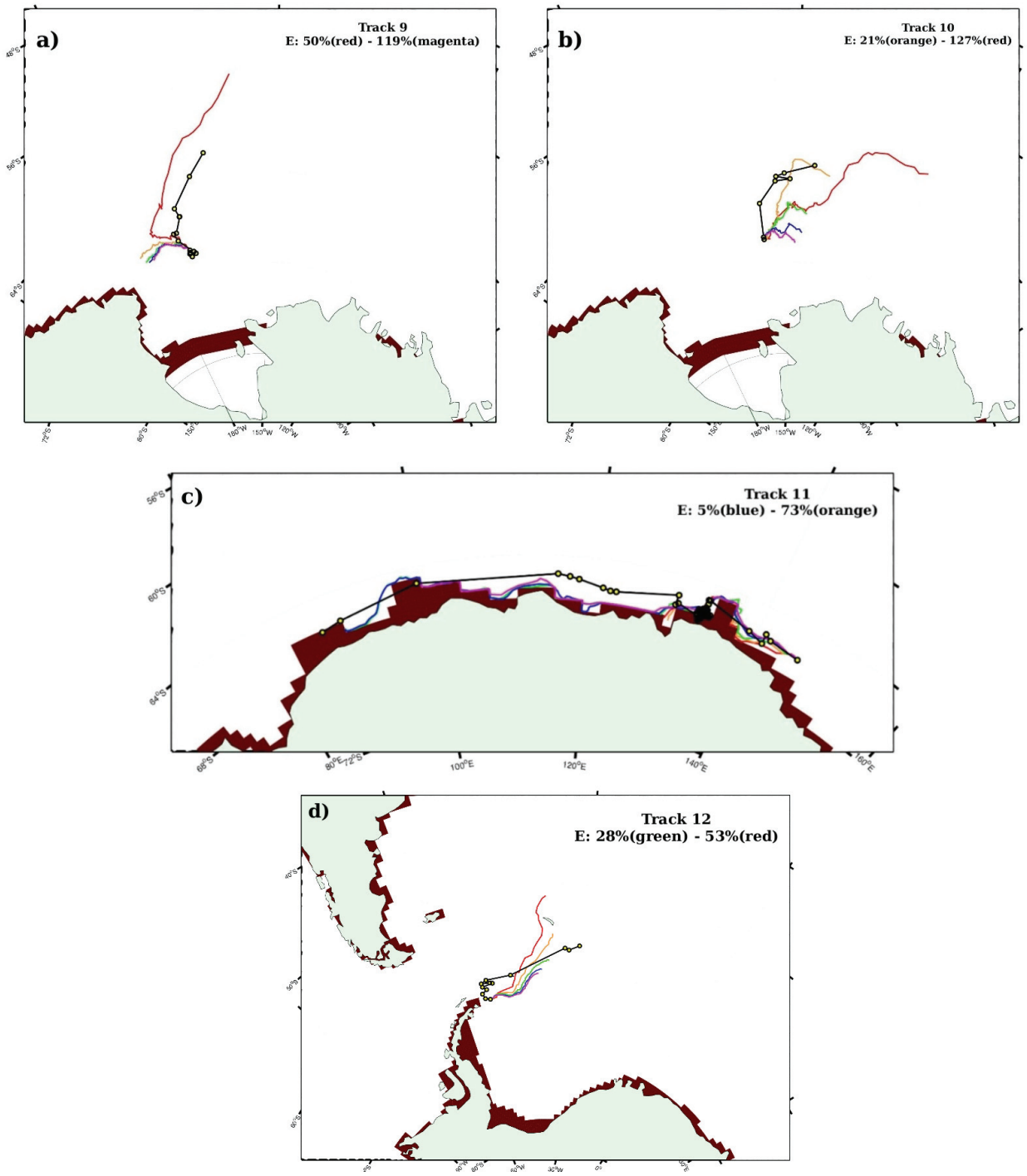

Figure 3–13: Same as figure 3–11 but for tracks 9 to 12(a-d). Track information is shown in table 3–4.

Track Length, Duration and Model Error. The length L_o of the successful tracks ranged from 290 km (Track #7) to 2942 (#2), and the duration, from 108 days (#8) to more than seven years (#11). On average, the track duration was close to two years, with a length of roughly 1500 km. The minimum distance error – defined as the error the most accurate modeled trajectory in one simulation – between modeled and observed track-endpoint ranged from five km to close to a thousand km. The minimum error E ranged from 0.9% to 50% of the total observed track length L_o. For the same set of simulations, the maximum distance error ranged from 154 km to almost 2900km, and E, from 53% to 177%. The correlations between track duration, and minimum and maximum model error E were found to be 0.12 and 0.38 respectively while the correlations between L_o and minimum and maximum E were -0.34 and -0.01 respectively. None of the correlations are significant at a 95% confidence level, indicating once again that the model error is not a function of either drift duration or length.

Location. Eight of the twelve successfully simulated tracks were located in the Weddell Sea, two were in the Ross Sea and one, along the Wilkes Land coastline. The dominance of Weddell sea tracks reflects the higher number of observed, and thus simulated, iceberg tracks in the region, and, perhaps, a better accuracy in the ocean model forcing in that area. More generally, all tracks except track #11, were located away from the coastline

Sensitivity to Initial Thickness There was no systematic bias in model performance with respect to iceberg thickness; the initial iceberg thickness of the most accurate modeled trajectory varied from one simulation to another. In the Weddell

Sea there was a tendency for the five icebergs launched in a given simulation to follow a similar path, with, however, an incremental shift to the left of the trajectory (for northward moving icebergs) of the path of thicker icebergs relative to thinner ones. The thicker icebergs also traveled slower (see discussion for details).

3.2.5 Simulations in which only the shape is reproduced

In six out of the twenty-nine simulations, the direction of the observed drift trajectories was well simulated but the timing was off. These six hindcasts are shown in figures 3–14 and 3–15.

Track Length, Duration and Model Error. The tracks ranged in duration from 225 days (track #14) to slightly more than 4 years (# 13). The length L_o of the modeled trajectories were between 1152 and 3565km. In all but one case (#16), the modeled iceberg was to slow, and arrived at the observed final position late. For all tracks except track #16, the time delay ranged from 200 days to close to 4000 days while the model error ϵ ranged between 89% and roughly 1700% of the total observed track duration. For track #16, the model iceberg was too fast by 44-55% which corresponds to an early arrival of 415-543 days.

Location. Four of the five simulations that were too slow compared to observations, were located along the Antarctic coastline. The fifth "slow" simulation was located slightly west of the middle of the Weddell sea. The simulation that was too fast was for an iceberg traveling in the open ocean from the eastern side of the Ross sea towards the Drake Passage.

Sensitivity to Initial Thickness. As in the previous subset of tracks, the model results show a tendency for thinner icebergs to travel the fastest within any

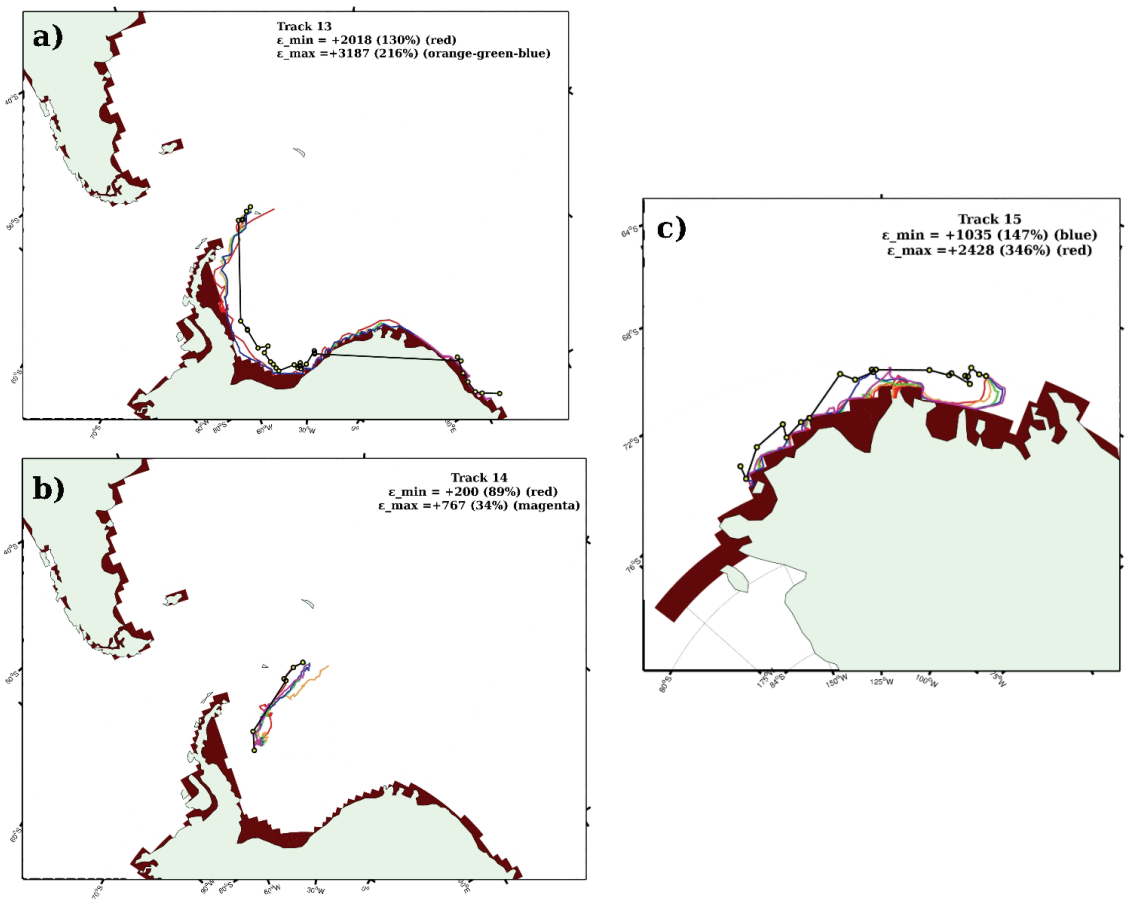

Figure 3–14: Same as figure 3–11 but for tracks 13 to 15 (a-c). Track information is shown in table 3–5.

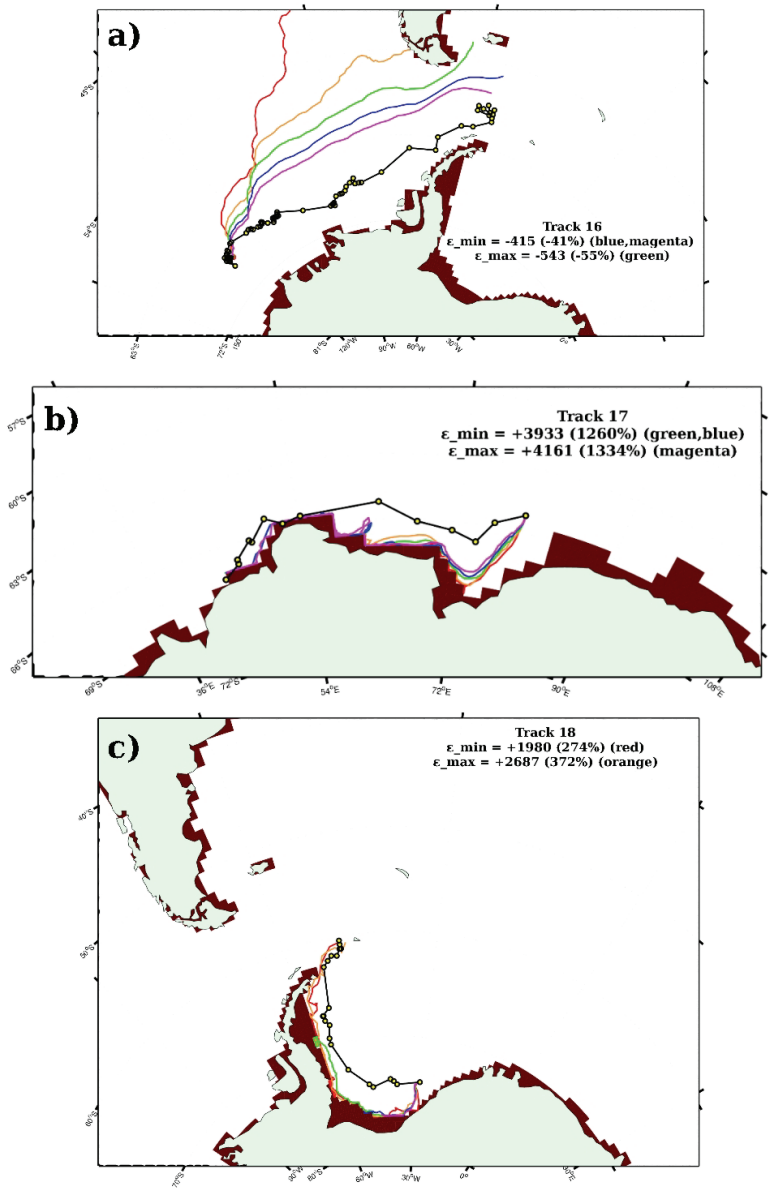

Figure 3–15: Same as figure 3–11 but for tracks 16 to 18 (a-c). Track information is shown in table 3–6.

given simulation, resulting in the smallest time delay for tracks that were too slow. In the same manner, the thicker icebergs resulted in the smallest model error ϵ for tracks that were too fast. Note however, that near the coast, the thinnest icebergs showed a greater propensity for colliding against and getting stuck in nooks of the model coastline. For this reason, in track #15, the thinnest iceberg arrived last at the observed trajectory endpoint.

3.2.6 Simulations in which the shape was not reproduced

In the remaining eleven cases, modeled iceberg of all five initial thicknesses started to move in the wrong direction from the start of the simulation (see figures 3–16 and 3–17. Initial details of these tracks is provided in table 3–7. The tracks ranged in duration from 109 days to slightly less than two years, with lengths L_o ranging from 534 to 1899 km. Note that the sub-sampling at a later time of observed trajectories that we failed to simulate, might have led to an artificial bias towards shorter track segments in this last category.

In all case the erroneous simulations were characterized by a strong spurious southward component in the motion of the modeled icebergs, which invariably resulted in the model icebergs colliding and adhering to the Antarctic coastline. In four cases, the unsuccessful modeled iceberg tracks were located in the southern portion of the Weddell Sea (track #19-22). There, the observed icebergs move northward and away from the coast while the modeled iceberg moved southward and then westward along the coastline. In one case, the model iceberg, after reaching the western side of the Weddell Sea (*i.e.,* the Antarctic Peninsula), started to move northward along the peninsula (track #19). Another set of failed simulations (tracks #23,24,26)

were co-located in the southern portion of the Ross sea, where model icebergs moved southwestward until they reached the coast, and then westward along the coast instead of moving northwestward as indicated by the observations. Similarly, in the simulation of track #27, the model iceberg failed to retroflect at the western edge of the Ross Sea, instead, moving south towards the coast, and then traveling westward along the coast. Hindcasts of tracks #27 and #28 show a recirculation of the model iceberg in Prydz Bay, and a subsequent collision with the coastline whereas both corresponding observed trajectory show fairly linear westward drift starting offshore of Prydz Bay and continuing parallel to the coastline. Finally, in the simulation of track #29, the iceberg collides with the coastline, which prevent the model iceberg from travel ling any further westward as seen in the observations.

3.2.7 Discussion

The IDM ability to forecast an individual iceberg drift trajectory was found to be independent of the track length and/or duration *i.e.*, the model error did not systematically increase with increasing simulation time. This suggests that the model error is due to random inaccuracies in the forcing/input data rather than to a faulty model formulation. Indeed, one expects an erroneous model formulation to lead to a systematic bias in the model results, and thus a model error increasing with increasing integration time. A probable source of the random model error is the simplification/assumptions made with respect to iceberg size, shape and, in particular, thickness. Model simulation shows that icebergs launched with initial thicknesses varying by as little as 50m can exhibit diametrically different behavior. More generally, results show that thinner icebergs tend to drift faster than thicker

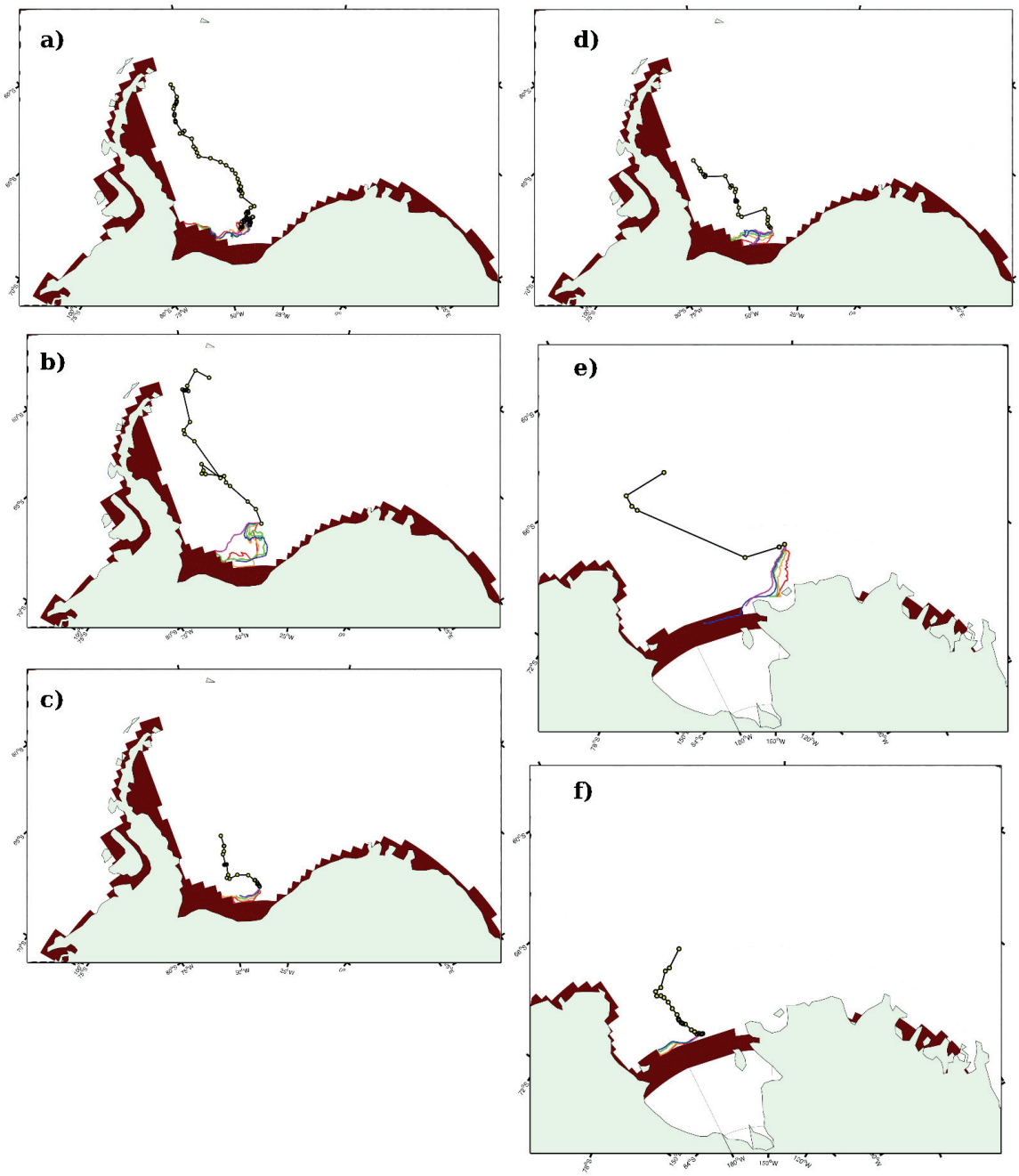

Figure 3–16: Same as figure 3–11 but for tracks 19 to 24 (a-f). Track information is shown in table 3–7.

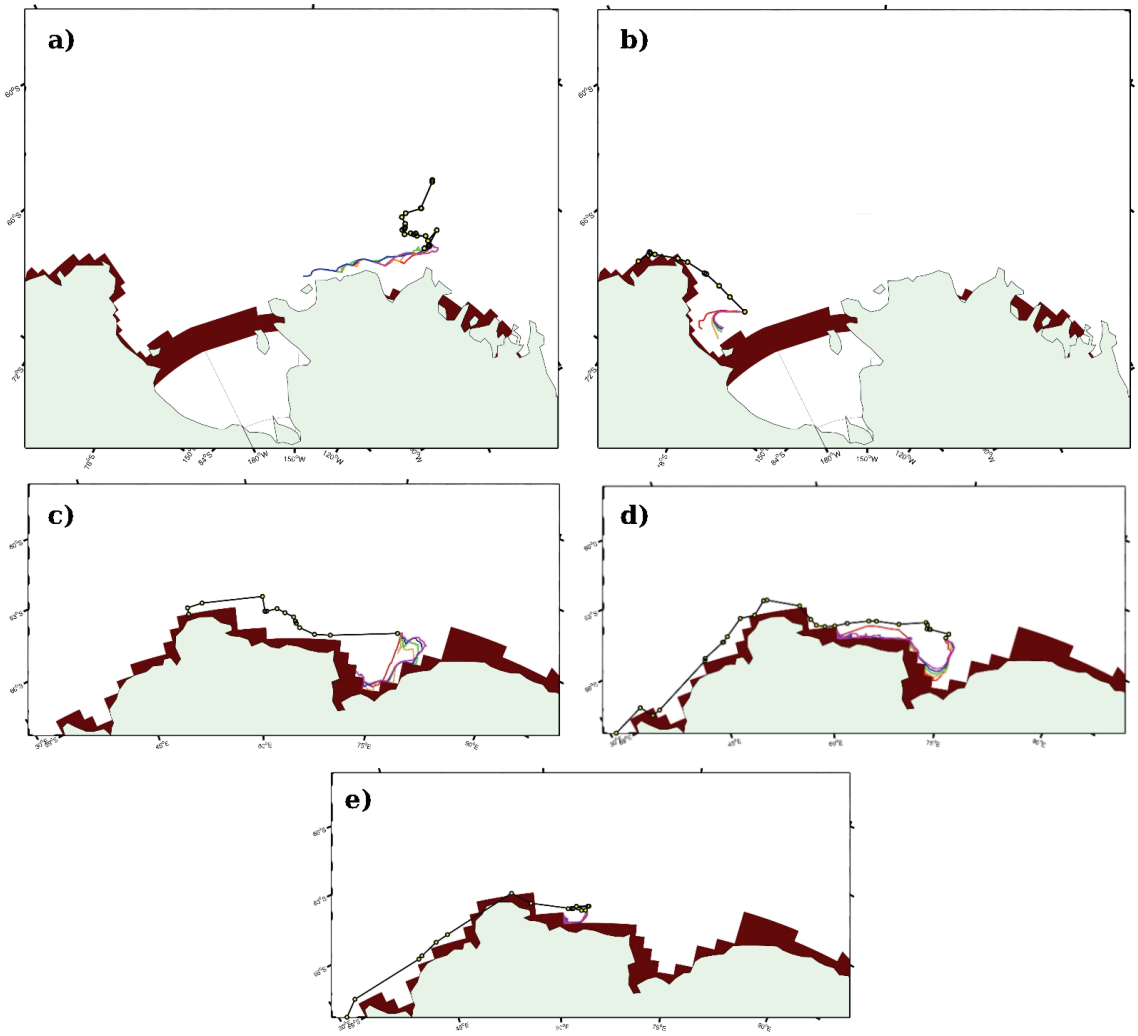

Figure 3–17: Same as figure 3–11 but for tracks 25 to 29 (a-e). Track information is shown in table 3–7.

ones and that their path tend to be deflected left of the path of thicker icebergs. This behavior is due to the fact that thinner iceberg have a greater proportion of their area/mass in the ocean Ekman layer. The Ekman layer refers to the surface ocean layer, where ocean currents are primarily forced by winds. In this boundary layer, the ocean currents turn and weaken with depth, so that the net water transport in the Ekman layer is roughly at 90°(to the left in the Southern Ocean Hemisphere) of the surface wind. The weakening of currents with depth in the Ekman layer and beneath the boundary layer also explains why thinner iceberg drift faster. Thus, an erroneous assumption of iceberg thickness can lead to a significant decrease in model performance compounded by the fact that individual model trajectories show a high sensitivity to year-to-year variation in forcing data (see figure 3–3) *i.e.,* a model iceberg that is too thin, and therefore drifts too fast, will be subject to untimely forcing, which will act to further increase the model error. Of course, it is also possible that inaccuracies in the model thermodynamic scheme lead to errors in model iceberg melt, size, and subsequently drift since the melt and momentum equations are strongly coupled through the iceberg thickness and the formulation of the Coriolis and drag forces.

At the same time, in our hindcast of giant iceberg drift tracks, model performance seems to be primarily a function of the location of the trajectory. For example, at the northern tip of the Antarctic Peninsula, observed iceberg tracks – for iceberg with horizontal dimension ranging from 14×3nm ($1.4 \times 10^8 \mathrm{m}^2$) to 45×30nm ($4.6 \times 10^9 \mathrm{m}^2$) – recorded in 1986,1989,1998,1999 and 2000 have all been well simulated. The modeled behavior of two iceberg launched offshore Prydz Bay showed the

same (erroneous) behavior even though they were launched four years apart. The fact that the spatial distribution of well and poorly modeled iceberg tracks does not change with time suggests that there are systematic errors in the fields used to force our IDM. Recall that the shape and timing of twelve individual iceberg drift tracks were successfully simulated. In six cases, the model reproduced the shape but not the timing of the observations, and in the eleven remaining simulations the icebergs moved in the wrong direction. Well simulated tracks were mostly located in the open ocean, away from the coast where the resolution of the forcing data is judged to be sufficient. Problematic tracks were, on the other hand, primarily located in coastal areas and in the southern portions of the Ross and Weddell seas. Poor model performance in these regions is probably due to inaccuracies in: (1) the model coastline, (2) the simulated coastal currents, (3) the Katabatic winds, and (4) the sea-ice parameters.

The complication arising from the poorly defined coastline are readily seen when observed drift trajectory (*e.g.,* from NIC) were overlaid on the ocean model grid, and some trajectories would be located on model "land". In the POP ocean model, ice shelves are treated as land, which results in spurious extension of the coastline northward. Moreover, a previous large-scale simulation of Antarctic iceberg drift (Gladstone et al., 2001) has shown that a difference of just 1°or 2° latitude in the iceberg position within the coastal current can make an iceberg move northward instead of continuing to drift westward in the coastal current. This is also seen in the observation data set near retroflection point, or in our simulation of track # 9 (see figure 3–13a) where a small difference in initial ice thickness leads to drastically

different trajectories. In addition, the 1979-2000 climatology calculated from the monthly-varying ocean fields (see Appendix A for climatology of forcing fields) used to force our IDM, show that the coastal current in the CCSM3.0 POP model itself are not resolved. Observations show that right next to the coast, the coastal currents can reach speeds of 25 cm s^{-1} due to the large horizontal pressure gradient in the region (Fahrbach et al., 1994). Further offshore, the current speed drops to an average of 5 cm s^{-1}. In the POP ocean model, the average surface current speed around Antarctica is not more than 5 cm s^{-1}. The model shows however a seasonal appearance of a stronger coastal current (with speed up to 15 cm s^{-1}) in certain regions around the continent, including along Wilkes Land, the eastern side of the Ross sea bay and near 0°. It is interesting to note that the only successfully modeled coastal track # 11, see figure 3–13(c)) in this study was along Wilkes Land, where the coastal current in the POP ocean model is best resolved.

The weaker coastal currents in our forcing fields also result in an underestimation of the coastal sea surface height gradient due to the weakening of the net southward Ekman water transport. In the iceberg momentum equation, this leads to a weakening of the sea surface tilt term which is responsible for pushing icebergs away from the coastline, partly explaining the (increased) tendency of model icebergs launched near the coast to collide with the continent.

Another probable source of model error is the sea-ice data used in the simulation. Lichey and Hellmer (2001), in his simulation of the drift of a giant iceberg through the Weddell Sea, has shown that in regions of high concentration and thickness of sea-ice, the sea-ice drag becomes the main driving force behind iceberg motion. The

author has also suggested that in order to accurately model iceberg drift in regions of multi-year sea-ice, one needs to allow the iceberg to be locked-in by ice, in which case the iceberg will drift with, and at the speed of sea-ice. In particular, the author has shown that the smaller the threshold for iceberg-sea ice locking, the more probable it is for an iceberg to retroflect in the middle-longitudes of the Weddell Sea rather than along its western boundary (the Antarctic Peninsula). In our study, all simulation of icebergs, that have been observed to retroflect in regions not immediately adjacent to the peninsula failed; the model icebergs instead moved southwestward towards the coastline (see tracks #19-22 in figure3–16(a-d)). Lichey and Hellmer (2001)'s study suggests that the failure of our model to simulate tracks #19-22 is due to the underestimation of the sea-ice drag term in the iceberg equation of motion, and perhaps, to the inability of sea-ice to lock-in an iceberg in our IDM. The ocean general circulation model used to derive the ocean forced had specified sea-ice concentrations, which were used to weight the heat and momentum fluxes between ocean and air. Thus, in regions of high sea-ice concentrations the transfer of momentum from wind to water, and thus the ocean surface currents were considerably inhibited. However, unlike in Lichey and Hellmer (2001) simulation, there was no sea-ice to "collect" the (northward) wind momentum that was not transferred to the ocean, which was simply "lost". By using the weakened ocean surface currents as an approximation of the drift speed of sea-ice, and because we assumed the ice thickness to be 1m everywhere, we also underestimated the sea-ice drag force. The inclusion of a more representative sea-ice thickness contribution will be considered in future work. Finally, note that southern portion of the Weddell Sea is characterized by multi-year

ice with thickness up to 6 m, which – if it was considered in our simulation – would have prevented the model iceberg to move as far south as simulated. Sea-ice drag and thickness underestimation also probably explains the modeled behavior of tracks #23-26 which failed to move northward (as seen in the observations) in the Ross sea.

Lastly, the model accuracy would benefit from a higher spatial resolution of the wind fields as well as a higher temporal resolution of ocean current fields, in which mesoscale weather systems and oceanic eddies (and tides) would be resolved. Gladstone et al. (2001) has shown that the addition of an extra wind forcing with the magnitude and on timescales of mesoscale weather systems induces small meanders in the iceberg drift trajectory, which allows a greater proportion of icebergs to leave the coastal currents. We speculate that – in addition to better resolved Katabatic winds and a stronger sea surface tilt term – mesoscale weather systems and ocean eddies in the forcing fields would also act to lower the proportion of icebergs that collide and adhere to the coastline. It is also possible that the presence of mesoscale forcing in our simulation would act to "slow down" model icebergs in the open ocean, which have been shown in this study to sometimes drift too fast, by introducing meanders in the simulated path. Indeed, Sodhi and El-Tahan (1980) have shown that the passage of a storm induces significant and almost immediate deviations in the drift pattern of icebergs on timescales as short as two days.

Other potential improvement to model accuracy include a more detailed thermodynamics scheme, and, in particular, a better representation of calving processes. Most recently, MacAyeal et al. (2007) have pointed out to the importance of ocean tides and collision *between* icebergs in governing giant iceberg motion. MacAyeal

et al. (2007) also theorizes that the inverse barometer effect – a relation between sea-surface elevation changes and local atmospheric pressure, whereas an upward deflection of the sea surface height will be observed below low atmospheric pressures and vice-versa – will result in giant icebergs moving up-slope sea-surface gradients rather than down-slope as previously believed under the pressure force resulting from the net pressure difference over the horizontal span of the iceberg. It would be of interest to assess the impact of the inclusion of these phenomena on model performance. The model results also shows good agreement with ship-based observations of the northernmost limits of Antarctic icebergs. These will be considered in future work.

CHAPTER 4
Conclusion

A Lagrangian dynamic-thermodynamic iceberg drift model (IDM) was developed, coded and validated against observations in the Southern Ocean. The momentum equation which governs the dynamics of a given iceberg includes the water, air, wave radiation as well as the Coriolis and the sea surface tilt forces. A similar balance of forces was first used by Smith (1993) with the parametrizations of the individual terms refined by Bigg et al. (1996, 1997), Lichey and Hellmer (2001) and Gladstone et al. (2001). The thermodynamic scheme of our model consists of empirical equations for basal melting (due to forced convection on the iceberg underside), lateral melting (due to buoyant convection) as well as erosional losses (due to forced convection) following work by El-Tahan et al. (1987) and Neshyba and Josberger (1980) amongst other.

The model is forced with monthly ocean and temperature fields from the CCSM3.0 POP ocean general circulation model, which has a horizontal resolution of 1.125° longitude × 0.65° latitude, and 40 vertical levels. The winds are taken from the same datasets used to force the ocean model, mainly the CORE CIAF datasets, based on the NCEP/NCAR reanalysis. The winds have a temporal resolution of 6 hours and a horizontal resolution of roughly 1.9°. Sea-ice concentrations from SSM/I data were read into the ocean model and used to weight the atmosphere-ocean momentum and heat. In our IDM, we use the SSM/I sea-ice fraction interpolated onto the ocean

model grid. The sea ice thickness is assumed to be 1 m everywhere, and the sea-ice velocity to be that of surface ocean currents.

We first asses the IDM's ability to simulate the large-scale patterns of Antarctic iceberg drift. The model reproduces the three main modes of Antarctic motion: (1) westward drift of icebergs in the coastal currents, (2) northward movement of icebergs at retroflection points, and (3) eastward drift of icebergs in the Antarctic Circumpolar Current. A more detailed model-data comparison of the retroflection points show that our IDM successfully simulates 4 of the 5 observed retroflection zones:(1) over the Kerguelen Plateau, (2) in the Ross sea, (3) off Adelie Land and (4) on the east flank of the Antarctic Peninsula . The fifth retroflection zone, located on the eastern boundary of the Weddell Sea gyre, is displaced further eastward in our simulation probably due to inaccuracies in the wind and ocean forcing fields of that region. The model also successfully reproduces the northward limit of Antarctic icebergs.

The model is then used to hindcast 29 individual iceberg drift trajectories located around the Antarctic continent, and of timescale on the order of years. The shape and timing of twelve of the twenty-nine tracks was successfully modeled with a model error in the 0.9-50% range. In six cases, the shape of the observed drift track was reproduced but the timing was off, and in the remaining eleven simulation the icebergs moved in the wrong direction. The model error is found to be independent of simulation length suggesting that the error is due to inaccuracies in the forcing data rather than in the physics of the model. In particular, model performance deteriorates in coastal areas and in the southern portions of the Weddell and Ross sea,

highlighting the need for higher resolution forcing data in these regions. We suggest that the model accuracy could be improved by the use of higher spatial (winds) and temporal (ocean) resolution data so that the model coastline is better defined and the Katabatic winds, mesoscale weather systems and ocean eddies are better resolved among other, as well as by the use of sea-ice thickness and velocity data from observations or an ocean general circulation model with a dynamic-thermodynamic sea-ice component.

In summary, we have shown the model's ability to simulate both the large-scale patterns of Antarctic iceberg drift and the motion of individual (giant) icebergs. Future work includes forcing the model with higher resolution data, and the inclusion of a sediment discharge subroutine in the model so that iceberg sedimentation in the Southern Ocean can be investigated. More precisely, we intend to use our IDM to constrain the interpretation of ice-rafted-debris records in the Southern Ocean, with the goal of exploring key questions about Antarctic ice sheet history including the timing of the initiation of the East Antarctic Ice Sheet as well as the onset of glaciation of the West Antarctic.

APPENDIX A
Climatology of forcing fields

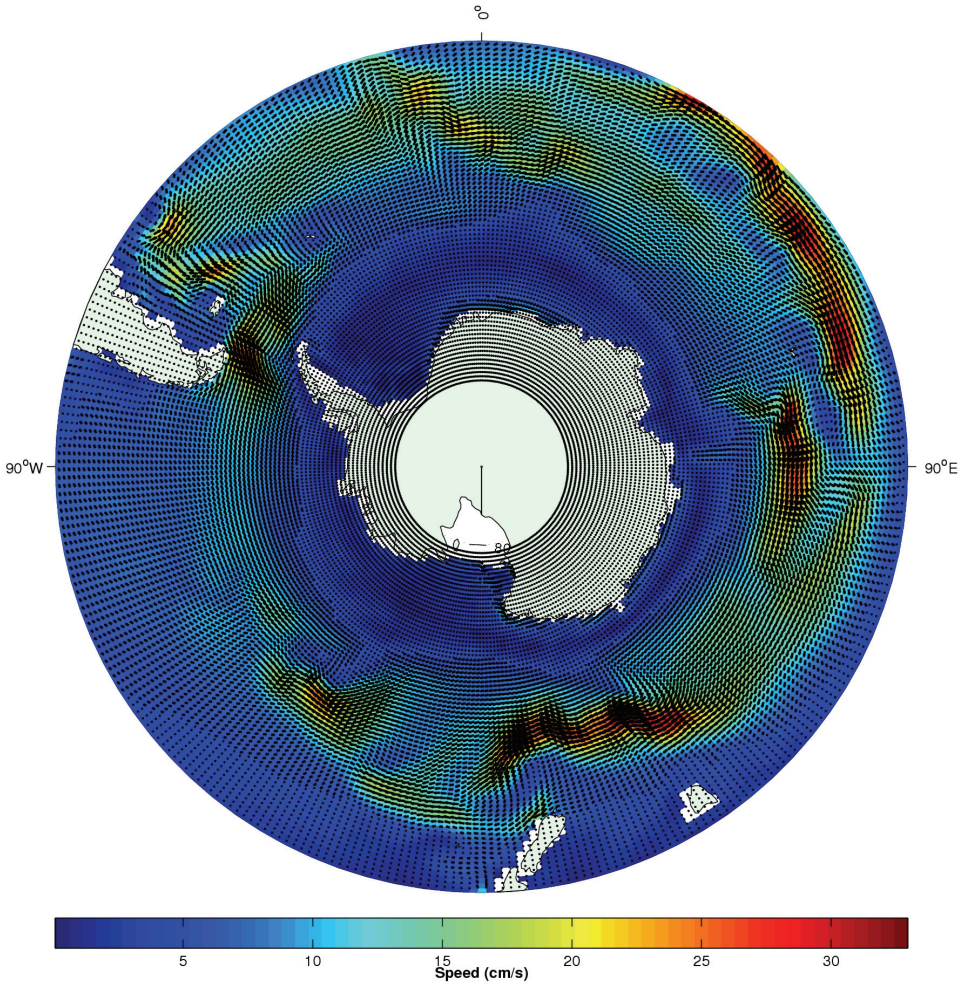

Figure A–1: February climatology (1979-2000) of surface ocean current.

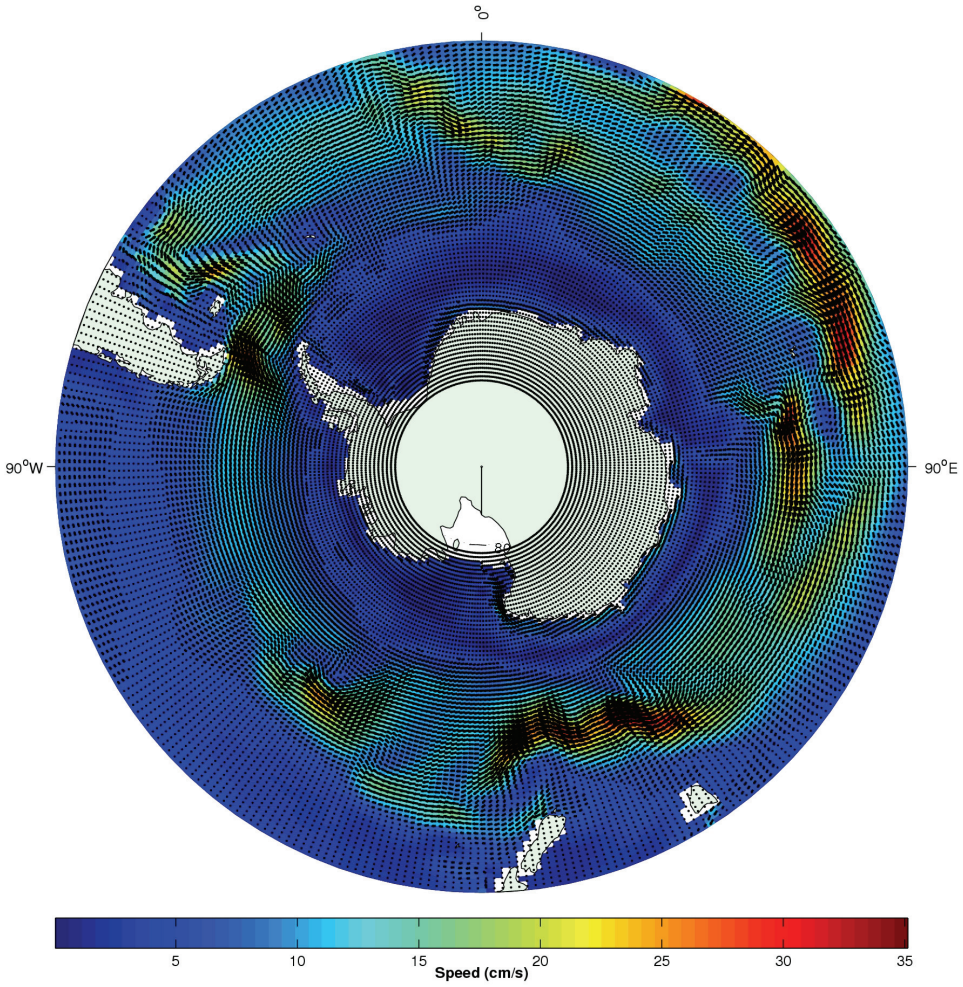

Figure A–2: September climatology (1979-2000) of surface ocean current.

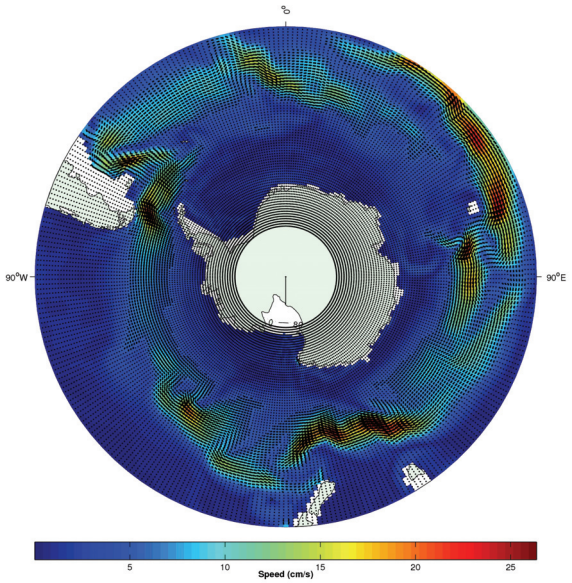

Figure A–3: February climatology (1979-2000) of ocean currents at depths of roughly 200m.

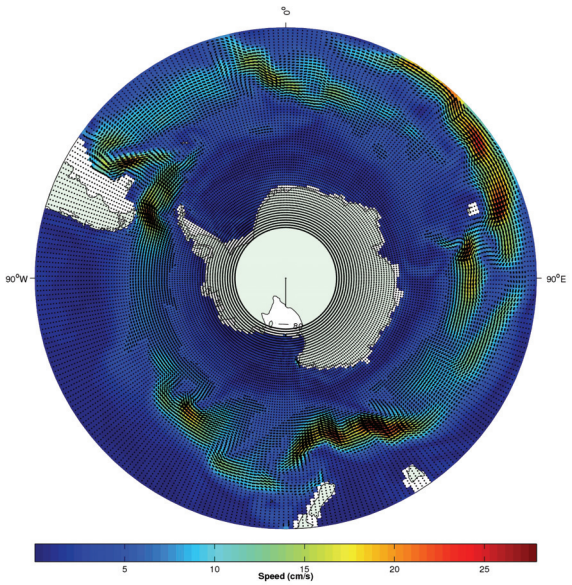

Figure A–4: September climatology (1979-2000) of ocean currents at depths of roughly 200m.

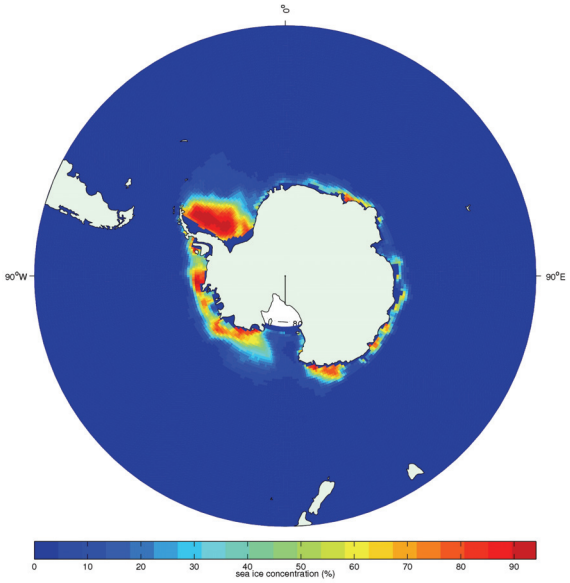

Figure A–5: February climatology (1979-2000) of sea-ice concentration.

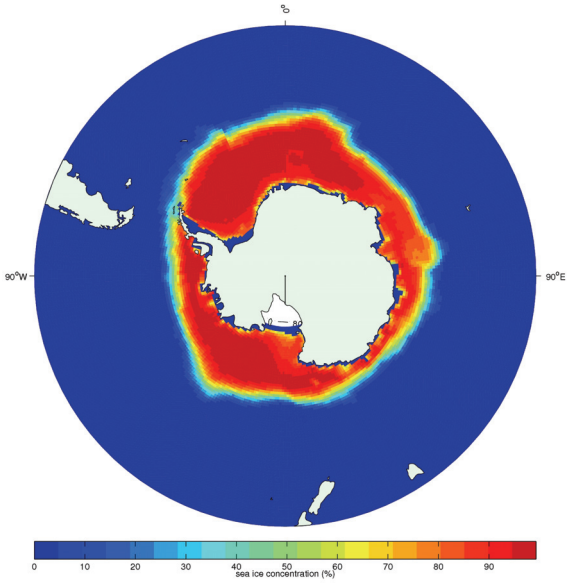

Figure A–6: September climatology (1979-2000) of sea-ice concentration.

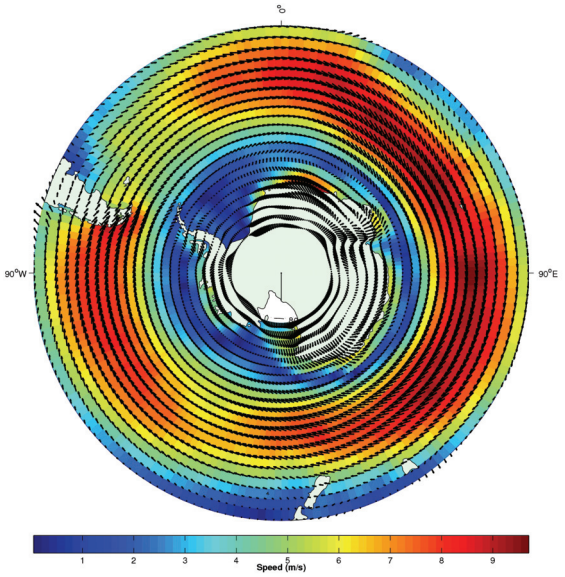

Figure A–7: February climatology (1979-2000) of 10m ASL winds.

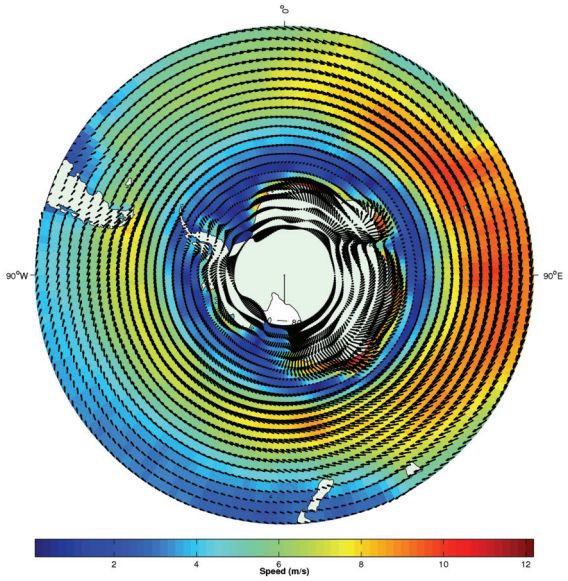

Figure A–8: September climatology(1979-2000) of 10m ASL winds.

REFERENCES

Anderson, J. B., E. W. Domack, and D. D. Kurtz, 1980: Observation of sediment-laden icebergs in Antarctic waters: implication to glacial erosion and transport. *J. Glaciol.*, **25**(93), 387–396.

Ballicater Consulting Ltd., 2005: Iceberg Observation Ilulissat, Greenland,*Contract Report Prepared for Canadian Ice Service, Environment Canada and Canadian Hydraulics Centre, National Research Council of Canada*,Ballicater Report 05-02.

Bigg, G. R., M. R. Wadley, D. P. Stevens, and J. A. Johnson, 1996: Prediction of iceberg trajectories for North Atlantic and Arctic Oceans. *Geophys. Res. Lett.*, **23**(24), 3587–3590.

Bigg, G. R., M. R. Wadley, D. P. Stevens, and J. A. Johnson, 1997: Modelling the dynamics and thermodynamics of icebergs. *Cold Reg. Sci. Technol.*, **26**, 113–135.

Bond, G., W. Broecker, S. Johnsen, J. McManus, L. Labeyrie, J. Jouzel, and G. Bonani, 1993: Correlations between climate records from North Atlantic sediments and Greenland ice. *Nature*, **364**, 143–147.

Bond, G., H. Heinrich, W. Broecker, L. Labeyrie, J. McManus, J. Andrews, S. Huon, R. Jantschik, S. Clasen, C. Simet, K. Tedesco, M. Klas, G. Bonani, and S. Ivy, 1992: Evidence for massive discharges of icebergs in the North Atlantic ocean during the last glacial period. *Nature*, **360**, 245–249.

Bourke, R. H. and R. P. Garrett, 1987: Sea ice thicknesses in the Arctic Ocean. *Cold Reg. Sci. Technol.*, **13**, 259–280.

Brey, T., D. Gerdes, J. Gutt, A. Mackensen, and A. Starmans, 1999: Growth and age of the Antarctic bryozoan *Cellaria incula* on the Weddell Sea shelf. *Antarctic Science*, **11**(4), 408–414.

Broecker, W., G. Bond, M. Klas, E. Clark, and J. McManus, 1992: Origin of the northern Atlantic's Heinrich events. *Clim. Dyn.*, **6**, 265–273.

Budd, W. F., T. H. Jacka, and V. I. Morgan, 1980: Antarctic iceberg melt rates derived from size distribution and movement rates. *Annals of Glaciology*, **1**, 103–112.

Clarke, G. K. C. and D. I. La Prairie, 2001: Modelling iceberg drift and ice-rafted sedimentation. In *Continuum Mechanics and Applications in Geophysics and the Environment*, Straughan, B., Greve, R., Ehrentraut, H., and Yongqi, W., editors. Springer-Verlag, New York, 183-200.

Death, R., M. J. Siegert, G. R. Bigg, and M. R. Wadley, 2006: Modelling iceberg trajectories, sedimentation rates and meltwater input to the ocean from the Eurasian Ice Sheet at the Last Glacial Maximum. *Paleogeo. Paleoclimato. Paleoeco.*, **236**, 135–150.

Dowdeswell, J. A. and E. K. Dowdeswell, 1989: Debris in icebergs and rates of glaci-marine sedimentation: observations from Spitsbergen and a simple model. *Journal of Geology*, **97**, 221–231.

Dowdeswell, J. A. and T. Murray, 1990: Modelling rates of sedimentation from icebergs. In *Glacimarine Environments: Processes and Sediments*, Dowdeswell, J.

and Scourse, J., editors. Geological Society Special Publication No 53., 121-137.

Drewry, D. J. and A. P. R. Cooper, 1981: Processes and models of Antarctic glaciomarine sedimentation. *Annals of Glaciology*, **2**, 117–122.

El-Tahan, M., S. Venkatesh, and H. El-Tahan, 1987: Validation and quantitative assessment of the deterioration mechanisms of Arctic icebergs. *J. Offshore Mech. Arctic Eng.*, **109**, 102–108.

Fahrbach, E., R. G. Peterson, G. Rohardt, P. Schlosser, and R. Bayer, 1994: Suppression of bottom water formation in the southeastern Weddell Sea. *Deep-Sea Research*, **41**, 389–411.

Gladstone, R. and G. R. Bigg, 2002: Satellite tracking of icebergs in the Weddell Sea. *Antarctic Science*, **14**(3), 278–287.

Gladstone, R. M., G. R. Bigg, and K. W. Nicholls, 2001: Iceberg trajectory modeling and meltwater injection in the Southern Ocean. *J. Geophys. Res.*, **106**(C9), 19,903–19,915.

Goda, Y., 2003: Revisiting Wilson's formulas for simplified wind-wave prediction. *J. Waterway, Port, Coastal, and Ocean Eng.*, **129**(2), 93–95.

Gupta, A. S. and M. H. England, 2006: Coupled ocean-atmosphere-ice response to variations in the Southern Annular Mode. *J. of Climate*, **19**(18), 4457–4486.

Gustajtis, K. A. and T. J. Buckley, 1978: A seasonal iceberg density distribution along the Labrador coast. In *Fourth International Conference on Port and Ocean Engineering under Arctic Conditions*, Muggeridge, D. B., editor, Memorial University of Newfoundland, St. John's, Newfoundland, 972-983.

Hanson, W. E., 1988: Operational iceberg forecasting concerns. In *OCEANS '88. 'A Partnership of Marine Interests'. Proceedings*, volume 2, 561-566.

Hay and Company Consultants Inc., 1986: Motion and impact of icebergs. Environmental Studies Revolving Fund Report 044, Ottawa. 136p.

Heinrich, H., 1988: Origin and consequences of cyclic ice rafting in the Northeast Atlantic Ocean during the past 130,000 years. *Quaternary Research*, **29**(2), 142–152.

Holland, D. and M. Maqueda, 2004: Modelling the impact of icebergs on the Southern Ocean freshwater budget and circulation. Obtained in January 2006 from D. Holland.

Huppert, H. E., 1980: The physical processes involved in the melting of icebergs. *Annals of Glaciology*, **1**, 97–101.

Intergovernmental Panel on Climate Change, 2007: Climate Change 2007: Impacts, adaptation and vulnerability: Working Group II Contribution to the Intergovernmental Panel on Climate Change Fourth Assessment Report Summary for Policymakers.

Jacka, T. H. and A. B. Giles, 2007: Antarctic iceberg distribution and dissolution from ship-based observations. *J. Glaciol.*, **53**(182), 341–356.

Jacobs, S. S., H. H. Helmer, C. S. M. Doake, A. Jenkins, and R. M. Frolich, 1992: Melting of ice shelves and the mass balance of Antarctica. *J. Glaciol.*, **38**(130), 375–387.

Job, J. C., 1978: Numerical modelling of iceberg towing for water supplies - A case study. *J. Glaciol.*, **20**(84), 533–542.

Keys, H. and D. Fowler, 1989: Sources and movement of icebergs in the South-West Ross Sea, Antarctica. *Annals of Glaciology*, **12**, 85–88.

Kristensen, M., V. A. Squire, and S. C. Moore, 1982: Tabular icebergs in ocean waves. *Nature* 669–671.

Kubat, I., M. Sayed, S. B. Savage, and T. Carrieres, 2005: An operational model of iceberg drift. *Int. J. Offshore and Polar Eng.*, **15**(2), 125–131.

Kubat, I., M. Sayed, S. B. Savage, T. Carrieres, and G. Crocker, 2007: An operational iceberg deterioration model. In *The Proceedings of The Seventeenth (2007) International Offshore and Polar Engineering Conference*, Chung, J. S., Hong, S. W., Nagata, S., Sarmento, A. J. N. A., and Koterayama, W., editors, volume 1, International Society of Offshore and Polar Engineers (ISOPE), Lisbon, Portugal.

Lichey, C. and H. H. Hellmer, 2001: Modeling giant-iceberg drift under the influence of sea ice in the Weddell Sea, Antarctica. *J. Glaciol.*, **47**(158), 452–460.

Long, D. G., J. Ballantyne, and C. Bertoia, 2002: Is the number of icebergs really increasing ? *EOS Trans. AGU*, **83**(42), pp. 469 & 474.

Löscher, B. M., H. J. W. de Baar, J. T. M. de Jong, C. Veth, and F. Dehairs, 1997: The distribution of Fe in the Antarctic Circumpolar Current. *Deep-Sea Res. II*, **44**(1-2), 143–187.

Lovenduski, N. S. and N. Gruber, 2005: Impact of the Southern Annular Mode on the Southern Ocean circulation and biology. *Geophys. Res. Lett.*, **32**, 4p. L11603, doi:10.1029/2005GL022727.

MacAyeal, D. R., J. Thom, M. H. Okal, K. M. Brunt, Y. Kim, and A. K. Bliss, 2007: Characteristics of tabular iceberg drift in the Southwestern Ross Sea, Antarctica.

Submitted to J. of Glaciology.

Marko, J. R. and D. B. Fissel, 1995: Comment on "On the deterioration of icebergs in the marginal ice zone"(Venkatesh et al., 1994). *Atmosphere-Ocean*, **33**(1), 187–189.

Marko, J. R., D. B. Fissel, and J. D. Miller, 1988: Iceberg movement prediction off the Canadian East coast. In *Natural and man-made hazards: International Symposium Proceedings*, El-Sabh, M. T. and Murphy, T. S., editors. Reidel, Dordrecht, 435-462.

Marshall, G. J., 2003: Trends in the Southern Annular Mode from observations and reanalyses. *J. of Climate*, **16**(24), 4134–4143.

Massom, R. A., 2003: Recent iceberg calving events in the Ninnis Glacier region, East Antarctica. *Antarctic Science*, **15**(2), 303–313.

Matsumoto, K., 1996: An iceberg drift and decay model to compute the ice-rafted debris and iceberg meltwater flux: Application to the interglacial North Atlantic. *Paleoceanography*, **11**(6), 729–742.

Matsumoto, K., 1997: Modeled glacial North Atlantic ice-rafted debris pattern and its sensitivity to various boundary conditions. *Paleoceanography*, **12**(2), 271–280.

Mellor, M., 1961: The Antarctic ice sheet. Number I-B1 in Cold regions science and engineering. U.S. Army Cold Regions Research and Engineering Laboratory, Corps of Engineers, Hanover, N.H.

Mountain, D. G., 1980: On predicting iceberg drift. *Cold Reg. Sci. Technol.*, **1**, 273–282.

Neshyba, S. and E. G. Josberger, 1980: On the estimation of Antarctic iceberg melt rate. *J. Phys. Oceanogr.*, **10**(10), 1681–1685.

Nielsen, J. W. and R. M. Dole, 1992: A survey of extratropical cyclone characteristics during GALE. *Mon. Wea. Rev.*, **120**(7), 1156–1168.

Oceans Ltd., 2004: Determination of iceberg draft and shape. *Submitted to the Canadian Hydraulics Centre*. PERD/CHC Report 20-75, Ottawa. 77p.

Oppenheimer, 1998: Global warming and the stability of the West Antarctic Ice Sheet. *Nature*, **393**, 325–332.

Orheim, O., 1980: Physical characteristics and life expectancy of tabular Antarctic icebergs. *Annals of Glaciology*, **1**, 11–18.

Orheim, O., 1988: Antarctic icebergs - production, distribution and disintegration (Abstract). *Annals of Glaciology*, **11**, 205.

Parish, T. R. and D. H. Bromwich, 1998: A case study of Antarctic Katabatic wind interaction with large-scale forcing. *Mon. Wea. Rev.*, **126**(1), 199–209.

Press, W. H., S. A. Teukolsky, W. T. Vetterling, and B. P. Flannery, 1992: *Numerical recipes in Fortran 77: The art of scientific computing*. Cambridge University Press, New York, 2 edition. See p.708-716.

Russell-Head, D. S., 1980: The melting of free-drifting icebergs. *Annals of Glaciology*, **1**, 119–122.

Savage, S. B., 2002: Aspects of iceberg deterioration and drift. In *Geomorphological Fluid Mechanics*, Balmforth, N. and Provenzale, A., editors, volume 582 of *Lecture Notes in Physics*. Berlin Springer Verlag, 279-318.

Scambos, T. A., C. Hulbe, M. Fahnestock, and J. Bohlander, 2000: The link between climate warming and break-up of ice shelves in the Antarctic Peninsula. *J. Glaciol.*, **46**(154), 516–530.

Schäfer-Neth, C. and K. Stattegger, 1999: Icebergs in the North-Atlantic: Modelling circulation changes and glacio-marine deposition. In *Computerized modeling of sedimentary systems*, Harff, J., Lemke, W., and Stattegger, K., editors. Springer, 63-78.

Schodlok, M. P., H. H. Hellmer, J. N. Schwarz, and T. Busche, 2005: On iceberg behaviour: observations, model results and satellite data. In *FRISP Report no. 16*, Forum for Research into Ice Shelf Processes, 19-25.

Silva, T. A. M., G. R. Bigg, and N. K. W., 2006: Contribution of giant icebergs to the Southern Ocean freshwater flux. *J. Geophys. Res.*, **111**(C03004), 1–8. doi:10.1029/2004JC002843.

Smith, S. D., 1993: Hindcasting iceberg drift using current profiles and winds. *Cold Reg. Sci. Technol.*, **22**, 33–45.

Smith Jr., K. L., B. H. Robinson, J. J. Helly, R. S. Kaufmann, H. A. Ruhl, T. J. Shaw, B. S. Twining, and M. Vernet, 2007: Free-drifting icebergs: hot spots of chemical and biological enrichment in the Weddell Sea. *Science*, **317**, 478–482.

Sodhi, D. S. and M. El-Tahan, 1980: Prediction of an iceberg drift trajectory during a storm. *Annals of Glaciology*, **1**, 77–82.

Soviet Antarctic Survey, 1966: *Antarctic Atlas.* Moscow. Plate 124.

Tchernia, P. and P. F. Jeannin, 1984: Circulation in Antarctic waters as revealed by iceberg tracks 1972-1983. *Polar Record*, **22**(138), 263–269.

U.S. Coast Guard, 2003: International Ice Patrol. [Accessed in 2006]. Availaible from World Wide Web: < http://www.uscg.mil/LANTAREA/IIP/home.html >.

van de Broeke, M. R., R. S. W. van de Wal, and M. Wild, 1997: Representation of Antarctic Katabatic winds in a high-resolution GCM and a note on their climate sensitivity. **10**, 3111–3130.

Venkatesh, S. and M. El-Tahan, 1988: Iceberg life expectancies in the Grand Banks and Labrador Sea. *Cold Reg. Sci. Technol.*, **15**, 1–11.

Venkatesh, S., D. L. Murphy, and G. F. Wright, 1994: On the deterioration of icebergs in the marginal ice zone. *Atmosphere-Ocean*, **32**(2), 469–484.

Vinje, T. E., 1980: Some satellite-tracked icebergs drifts in the Antarctic. *Annals of Glaciology*, **1**, 83–87.

Wadhams, P., 2000: *Ice in the ocean.* Gordon and Breach Science Publishers, 239-272.

Warnke, D. A. and J. Richter, 1970: Sedimentary petrography of till from a floating iceberg in Arthur Harbor,Antarctic Peninsula. *Rev. Geogr. phys. Geol. dynam.*, **XII**(5), 441–448.

Weeks, W. and M. Mellor, 1978: Some elements of iceberg technology. In *Iceberg Utilization; Proceedings of the first international conference and workshops on iceberg utilization for fresh water production, weather modification and other applications*, Husseiny, A. A., editor, Iowa State University, Ames, Iowa, 45-98.

Weeks, W. F. and W. J. Campbell, 1973: Icebergs as a fresh-water source: an appraisal. *J. Glaciol.*, **12**(65), 207–233.

White, F. M., M. L. Spaulding, and L. Gominho, 1980: Theoretical estimates of the various mechanisms involved in iceberg deterioration in the open ocean environment. Technical Report CG-D-62-80, U.S. Coast Guard. p. 126.

Wikipedia, 2007: Beaufort scale [online]. [Accessed 4 April 2007]. Available from World Wide Web: < http://en.wikipedia.org/wiki/Beaufort_scale >.